2ND LSA SAF WORKSHOP

INSTITUTO DE METEOROLOGIA

LISBON, PORTUGAL

8-10 MARCH 2006

SESSION 4 – Applications of LSA SAF Products

OPERATIONAL SNOW MAPPING WITH METEOSAT-8 SEVIRI AT METEOSWISS

Martijn de Ruyter de Wildt [1, 2] and Jean Quiby [2]

[1] Institute of Geodesy and Photogrammetry, ETH Zurich
ETH Hoenggerberg, 8093 Zurich, Switzerland
[2] MeteoSwiss
Krähbühlstrasse 58, Postfach 514, 8044 Zurich, Switzerland

ABSTRACT

In this paper we describe how Meteosat-8 SEVIRI data are used for snow mapping at MeteoSwiss. Of particular interest for snow mapping is the high temporal frequency of SEVIRI, which makes it possible to retrieve information about surface snow cover in near real-time and to improve image classification by analysing the behaviour of pixels in time. With spectral information alone, not all clouds can be discriminated from snow, because the spectral signatures of clouds and snow partly overlap. However, many cloudy pixels display a higher variability in time than cloud-free pixels and this property can be used to detect them. When temporal information is used in addition to spectral information, the classification accuracy of images from several test periods is significantly improved.

1. INTRODUCTION

Snow cover influences several processes that occur at or near the Earth's surface. It affects the exchange of energy and moisture between the surface and the atmosphere and is an important aspect of the hydrological cycle. Furthermore, snow cover extent is an indicator of climatic change and affects many human activities. Information about the surface snow cover is therefore important for studies and applications in many disciplines, including Numerical Weather Prediction (NWP), hydrology and climatology. A valuable tool for detecting snow cover is remote sensing, because it allows us to monitor large areas of the Earth at regular time intervals.

Different satellites sensors have been used for snow mapping. NOAA AVHRR combines a repeat time of several hours with a spectral resolution of 1 km at nadir, which has made it a popular sensor for snow mapping (e.g. Ebert, 1987; Gesell, 1989; Allen et al., 1990; Baum and Trepte, 1999). Another sensor that is suitable for snow mapping is MODIS, on board of NASA's Terra and Aqua satellites. It has 36 narrow spectral bands and can be used to produce daily snow maps with a spatial resolution of 500 m (Hall et al., 2002). Other sensors with which snow cover has been mapped are Landsat TM (e.g. Dozier, 1989) and Terra/Aqua ASTER (Logar et al., 1998; Welch et al., 1999). The only geostationary satellites that, until recently, could be used for detecting surface snow cover were the Geostationary Operational Environmental Satellites (GOES) (Romanov et al., 2000; Romanov et al., 2003). From the many images that are acquired during a day, the authors made a composite daily image by retaining, for each pixel, only the warmest (i.e. the most cloud-free) instantaneous value, and then classified this composite image. Another geostationary satellite instrument, MVIRI (Meteosat Visible and Infrared Imager) on board of the Meteosat satellites, has not been used for snow mapping because is has only two channels that detect surface radiation (visible and infrared).

In 2002 the first Meteosat Second Generation satellite (MSG-1) was launched by the European Organisation for the Exploitation of Meteorological Satellites (EUMETSAT). This satellite, now known as Meteosat-8, carries the Spinning Enhanced Visible and Infrared Imager (SEVIRI), which is the first geostationary instrument that measures at all bandwidths that are of use for snow mapping. Furthermore, it has a temporal resolution of 15 minutes, whereas its predecessors on board of the previous Meteosat satellites have a temporal resolution of 30 minutes. It therefore allows a good separation between snow and clouds and makes it possible to monitor surface snow cover on a very regular basis. This study presents results of a EUMETSAT fellowship that aims at developing an automated snow mapping algorithm for Meteosat-8 SEVIRI data. This algorithm is intended for delivering snow cover data in near real-time to the operational mesoscale NWP model of MeteoSwiss, the Alpine Model (aLMo). An important aspect of the project is to use the high temporal resolution of the SEVIRI data for snow mapping. Also, the algorithm must deal with the specific difficulties that occur over alpine terrain, and in this respect it differs from the SEVIRI snow mapping algorithm that has been developed by EUMETSAT's Nowcasting SAF (López Cotín, 2005).

The high frequency allows us to reduce cloud obscuration of the ground by detecting all cloud-free periods longer than 15 minutes and to retrieve information about the surface on a very frequent basis. Also, the high frequency can be used to monitor dynamic processes and the behaviour of pixels in time. This is of interest for detecting clouds, which can have a similar spectral signature as surface snow and may not always be detectable with spectral information alone. However, irrespective of their spectral signature, clouds often display a much more dynamic behaviour than the earth's surface. In this paper we describe the cloud detection algorithm, which uses temporal information in addition to spectral information to discriminate clouds from snow covered regions.

2. DATA

SEVIRI continuously monitors the entire earth disk with a frequency of 15 minutes and has 12 spectral channels, 8 of which can be used for monitoring the surface (table 1). Channel 12 is a high resolution visible (HRV) channel, which has a resolution of 1 km at the sub-satellite point. All of the other channels have a spatial resolution of 3 km at the sub-satellite point. The area of interest is central Europe, which is the model domain of aLMo.

For testing and validation we selected the following six days: March 8th-10th, 2004, January 19th, 2005 and February 23rd-24th, 2005. On these days, all mountainous regions of Europe were covered with snow, as well as many other parts of Europe. The weather was variable, and clouds, some of them containing ice particles, bare land and snow covered land were all well represented over Europe.

channel	central wave length (µm)	description	divergence parameters for equation 1 with 3, 5, 7 and 9 images			
			3	5	7	9
1	0.64	visual	0.712	0.749	0.752	0.740
2	0.81	visual	0.702	0.734	0.731	0.709
3	1.6	near infrared	0.737	0.729	0.702	0.671
4	3.9	solar + terrestrial infrared	0.613	0.639	0.648	0.655
5	6.2	infrared (water vapour absorption)	0.380	0.408	0.409	0.402
6	7.3	infrared (water vapour absorption)	0.574	0.601	0.603	0.597
7	8.7	Infrared	0.678	0.700	0.693	0.679
8	9.7	infrared (ozone absorption)	0.582	0.619	0.626	0.622
9	10.8	Infrared	0.657	0.679	0.674	0.662
10	12.0	Infrared	0.637	0.658	0.654	0.642
11	13.4	infrared (CO_2 absorption)	0.588	0.619	0.621	0.615
12	HRV	high resolution visual broadband	0.731	0.767	0.759	0.733

Table 1: The twelve SEVIRI channels and average divergence parameters for the separation of snow cover and clouds containing ice particles.

3. METHOD

As a basis for image classification we use several spectral thresholds tests that are in common use. These tests are used to designate each pixel to one of three classes: cloud, snow or bare land. Subsequently, the classification result is subjected to a temporal test, which maks pixels that display a high temporal variability. This test is only applied to pixels that may have been misclassified as clear by the spectral tests, which are undetected ice clouds and cloud shadows.. The last step of the classification procedure is a temporal consistency test, with which any remaining undetected ice clouds are filtered out from the snow pixels. A snow pixel is rejected when, for 2 or more pixels in the surrounding block of nine pixels, it was classified as cloud in the previous image and in the next image. The classification scheme is shown in Figure 1.

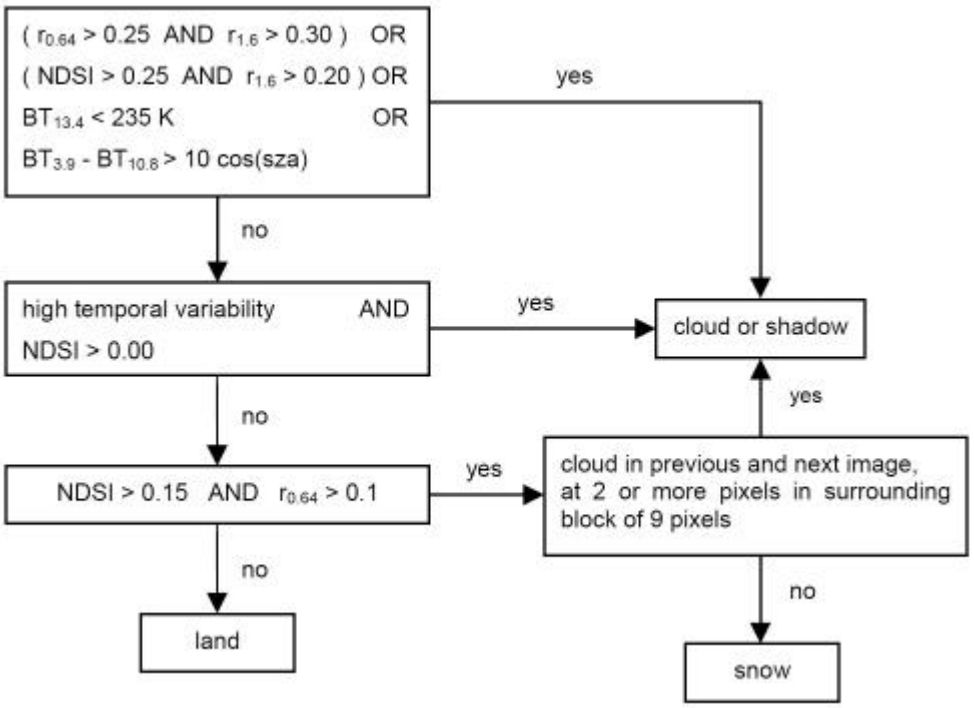

Figure 1: Flowchart for classification.

3.1. Spectral classification

Existing algorithms for spectral classification of snow use several satellites and sensors. These sensors have channels in the same spectral regions, although the exact bandwidths vary. For some of the spectral threshold tests we therefore empirically adapted the thresholds. To avoid problems that are caused by a low solar zenith angle (sza), pixels with a sza above 80° are discarded. A pixel is masked as cloud when at least one of the following threshold tests is passed:

- r0.64 > 0.25 and r1.6 > 0.30 (e.g. Dozier, 1989; Riggs and Hall, 2002). The 0.64 µm test separates bare ground from snow and clouds. Many clouds can be distinguished from snow in the 1.6 µm channel, which is sensitive to the phase of the clouds (e.g. Dozier, 1989). However, this channel can not separate clouds with many ice crystals from snow.
- r0.64 > 0.25 and NDSI > 0.20, where NDSI stands for Normalised Differential Snow Index (Dozier, 1989; Hall et al., 1995). This index equals (r0.64-r1.6)/(r0.64+r1.6) and enlarges the contrast between snow and bare ground, as snow has a higher r0.64 and a lower r1.6

than snow free land. The NDSI can also be used to mask clouds, as many clouds display a rather high NDSI (Riggs and Hall., 2002).
- BT3.9 - BT10.8 > 10 cos(sza). This thermal difference has been used by several authors (e.g. Allen et al., 1990; Baum and Trepte, 1999; Riggs and Hall, 2002). The threshold depends on the solar zenith angle (López Cotín, 2005), because the SEVIRI 3.9 µm channel not only detects terrestrial radiation, but also a small amount of solar radiation.
- BT13.4 < BT13.4,min (Riggs et Hall, 2002). This test separates very cold clouds from snow.

Pixels that are not classified as cloudy, are checked for the presence of snow by two other spectral tests. A cloud free pixel is classified as snow when both of the following conditions are fulfilled:

- NDSI > 0.15
- r0.64 > 0.1. This criterion ensures that very dark surfaces, which can cause the denominator of the NDSI to be very small, are not classified as snow (Hall et al., 2002).

3.2. **Temporal classification**

As a measure of temporal variability we use the standard deviation in time, averaged over each pixel and its eight neighbours. Several other measures were also tested, but were found to be less suitable. For a pixel in channel m of the current image (time t=0), this temporal standard deviation is:

$$d_m = \sum_{i=-1}^{1} \sum_{j=-1}^{1} w_{i,j} \sqrt{\frac{1}{2n} \sum_{t=-n}^{n} \left(I_{m,t} - \langle I_m \rangle \right)^2} \qquad (1)$$

where I is the radiation intensity (expressed as reflectance, r, or as brightness temperature, BT), n is the number of images before or after the current image and 2n is the number of time steps. i and j are spatial indices in the x and y directions, respectively and w is the weight of each pixel. For the central pixel (i=0, j=0) we use w=2, for the neighbouring pixels in the x- and y-directions w=1 and for the neighbouring pixels in the diagonal directions $w=1/\sqrt{2}$. Although this classifier considers the eight surrounding pixels, it does not quantify spatial variability, and can therefore be regarded as a quasi three-dimensional classifier.

We found the optimal number of time steps for separating clouds from surface snow by calculating the following divergence parameter (Wu et al., 1985):

$$D_m = \frac{\left| \langle d_{m,cloudy} \rangle - \langle d_{m,snow} \rangle \right|}{\sigma_{m,cloudy} + \sigma_{m,snow}} \qquad (2)$$

where $\langle dm \rangle$ is the mean value and σm the standard deviation of dm for all pixels in an image that belong to the classes 'cloudy' and 'snow'. For all images from the six days of intensive observation we computed the mean value of Dm for each channel m and for several values of n. This was also done for the HRV channel, which has exactly nine pixels in each normal (low) resolution pixel. Values of dHRV for the low resolution grid were obtained by adding all nine high resolution values.

We found higher divergences for the reflectance channels than for the infrared channels, which is caused by the often static behaviour of water clouds in the infrared channels. When we exclude water clouds from the analysis by omitting all cloudy pixels with a near infrared reflectance above 0.5, the divergences for the infrared channels resemble those for the solar channels more closely. These divergences are shown in table 1. The highest divergence is found for the reflectance in the HRV channel, which detects the most detailed information. The other three solar channels also

display high divergences, whereas the infrared channels display slightly lower divergences. As might have been expected, the lowest values are found for the water vapour and ozone absorption channels at 6.2, 7.3 and 9.7 μm. The first two channels measure water content in the upper troposphere and the latter channel is influenced by ozone in the lower stratosphere. Changes in these quantities can occur independently of cloudiness at lower levels, which is why we do not use these three channels for temporal detection of clouds. Larger divergences are found for all other infrared channels, which detect significant amounts of information from low atmospheric levels. Thus, we use all channels except the water vapour and ozone absorption channels for temporal detection of clouds.

Table 1 shows that snow and ice clouds are best separated when 5 successive images are used to compute the temporal standard deviation with equation 1 (i.e. with n=2). Shorter time series obviously include too little temporal information. On the other hand, the use of longer time series will increase the temporal variability of pixels that are cloud free in the current image and cloudy several time steps earlier or later (or vice versa).

4. RESULTS

For analysing the performance of the algorithm, we focus on March 10th, 2004, because on this day clouds were present that were difficult to distinguish from snow. For visual discrimination between snow and optically thick ice clouds, one can make an RGB combination of different channels and view animated time series of this RGB image. Because of their dynamic behaviour, many clouds are clearly recognisable to the human eye in such animations. A combination of channels that is useful for this purpose is made from three spectral features that are important for snow mapping: r0.64, r1.6 and BT3.9 - BT10.8. Examples of the RGB animations are available on the project web-site: www.photogrammetry.ethz.ch/research/snow/index.html.

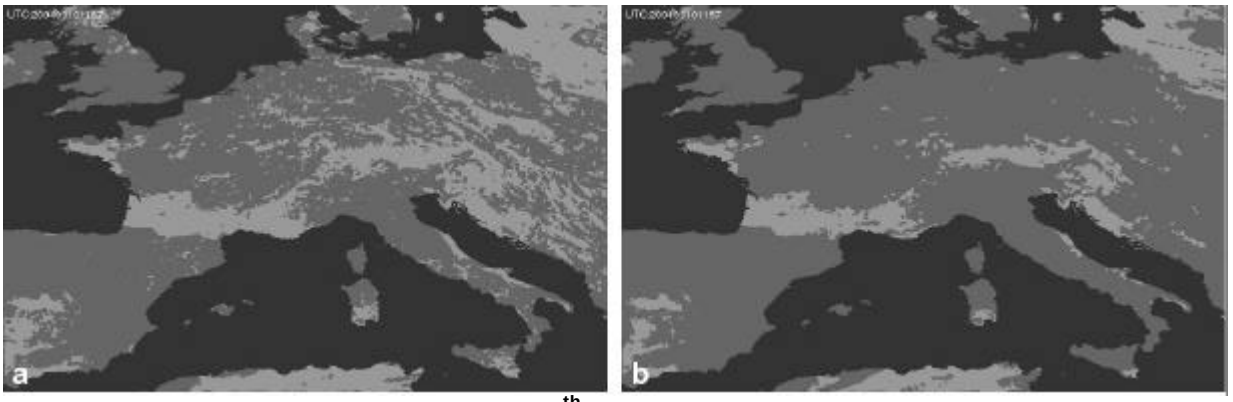

Figure 2: Temporal cloud mask for March 10th, 2004, starting scan time 11:45. (a) only for $r_{0.64}$ and without spatial consistency filtering and (b) for all used channels, with spatial consistency filtering. Light grey pixels are cloud free, dark grey pixels are cloudy.

Figure 2 shows that most clouds can be effectively masked with the temporal cloud masking algorithm. When the temporal variability in only one channel is thresholded, many clouds are masked although numerous gaps remain (Figure 2a). The result strongly improves when all single channel cloud masks are stacked and a spatial consistency filter is applied that masks all pixels that are surrounded by at least 6 cloudy pixels (Figure 2b). The classification result for the same image is displayed in Figure 3a. Visual inspection reveals that there are no clouds that are misclassified as snow. On the other hand, too many cloudy pixels are detected near cloud edges

and over regions with broken cloud cover. This is caused by the temporal classification method: pixels that are cloud free in the current image, may be cloud covered in the preceding or in the succeeding images. In these cases the temporal variability of these pixels will be high and they will we masked as cloud. When we omit the temporal classification and only apply a spectral classification (Figure 3b), more snow covered pixels are classified correctly (e.g. over the Alps and over eastern Europe), but also a considerable number of cloudy pixels is now classified as snow.

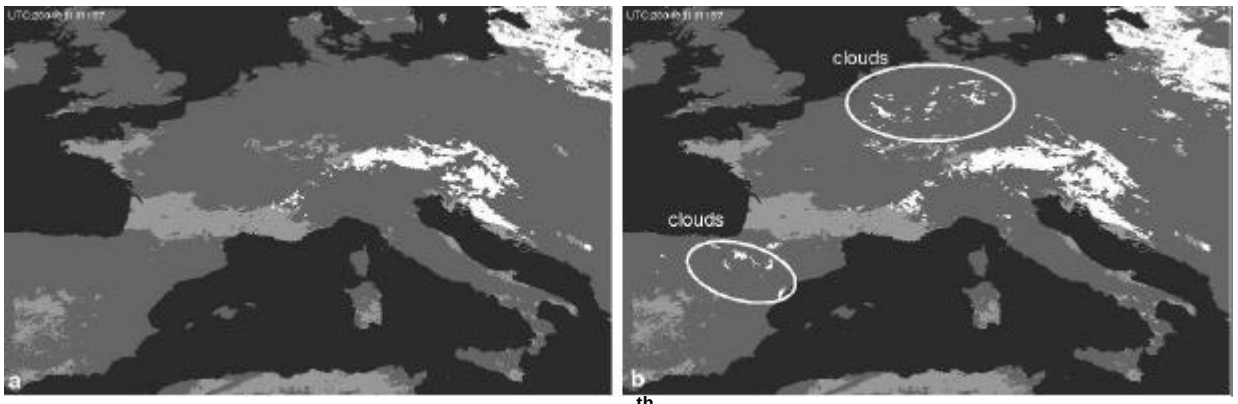

Figure 3: Instantaneous snow maps for March 10th, 2004, starting scan time 11:45. White pixels represent snow, dark grey pixels clouds and light grey pixels bare land. Plot a shows the result for the full classification method, including the temporal classification. For plot b only the spectral classification was used.

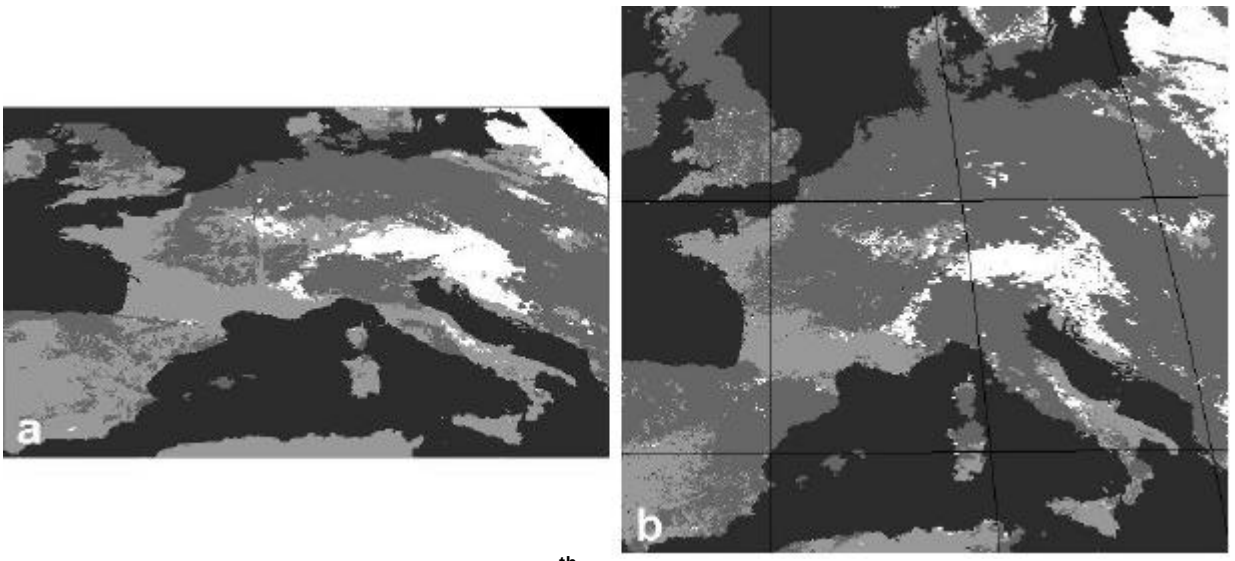

Figure 4: Composite snow maps for March 10th, 2004. (a) Meteosat-8 SEVIRI. (b) MODIS, as obtained from the MODIS Land Quality Assessment Site (landweb.nascom.nasa.gov/cgi-bin/browse/browse.cgi).

The large cloud-covered area which is visible in Figure 3 can be reduced by combining several successive snow maps into a composite map. For making daily composite snow maps, we use the following rules. When a pixel is cloud free in one or more of the instantaneous snow maps, it will be cloud free in the composite snow map. This means that only pixels that are cloudy in all instantaneous images, are cloudy in the composite map. A pixel will be snow covered in the composite map, when it is classified as snow in at least one of the instantaneous images. The result for March 10th, 2004, is shown in Figure 4a. Now, much less pixels are cloud covered and more surface snow cover is visible.

The composite snow map can be validated qualitatively by comparing it with similar snow cover products. One such product is the MODIS daily composite snow cover product (Hall et al., 2002). Figure 4b displays this daily composite for March 10th, 2004. The most noticeable difference with the SEVIRI snow map is the larger part of the surface that was not visible on this day due to cloud cover. The cause of this difference is the smaller number of MODIS images that are available, compared to the number of SEVIRI images. Another difference between the two snow maps are the small isolated snow patches surrounded by clouds in the MODIS product, which do not occur in the SEVIRI product. An analysis of the animated time series of SEVIRI RGB's revealed that these pixels partly correspond to surface snow cover and partly to ice clouds. All of these pixels are classified as clouds by the temporal component of the SEVIRI algorithm, because these pixels or neighbouring cloudy pixels display temporal variability. Thus, the temporal classification of the SEVIRI algorithm overestimates the amount of clouds, but by doing so it misses no ice clouds.

5. DISCUSSION AND CONCLUSIONS

The advantage of geostationary satellites over polar orbiting satellites is the very high temporal frequency with which their instruments can monitor the surface. This property can be used to monitor changes that occur on a time scale of minutes to hours. For monitoring the earth's surface, it is important that geostationary satellite data show the movement of clouds and that in a series of images all cloud-free moments that occur are observed. Thus, when single images from geostationary satellites are combined into a composite image, cloud cover is reduced (e.g. Romanov et al., 2000; Romanov et al., 2003). The high temporal frequency can furthermore be used to improve the detection of clouds in single images. Many clouds are more variable in time than the surface and this property can be used to identify them. In particular, this is useful for detecting relatively warm and optically thick ice clouds. These clouds cannot be distinguished from snow with spectral threshold tests alone, because their spectral properties overlap with those of snow.

The temporal algorithm slightly overestimates the number of cloudy pixels, but the pixels that are classified as cloud-free, have a high reliability. The resulting snow map can therefore be considered as conservative, in the sense that the probability of rejecting a correct snow pixel (type I error) is larger than the probability of accepting a false snow pixel (type II error). Fortunately, the number of cloudy pixels can be strongly reduced by combining several instantaneous snow maps in one composite snow map. Also, for NWP models this conservatism is desirable, as a type I error has less severe consequences than a type II error. When the surface snow cover is obscured by clouds, the snow cover of the previous period or the modelled snow cover may be used, whereas erroneous snow cover will introduce errors in the NWP model computations.

A validation of the results has been performed by comparing them with the MODIS snow product and by visual inspection of animations of RGB-combinations. We consider such a visual inspection as a reliable way for qualitative validation, because the animations, in contrast to single images or RGB-combinations, reveal the dynamic behaviour that many clouds display. A more elaborate quantitative validation with in situ snow observations and other satellite images (e.g. MODIS, MISR, AVHRR) is in preparation. We will also use additional periods for testing and validation, in order to see how the algorithm performs under other meteorological conditions. Furthermore, the algorithm has room for several improvements, such as corrections for atmospheric influence and anisotropy, the inclusion of surface topography, the detection of fractional instead of binary snow cover and the inclusion of quality flags.

6. ACKNOWLEDGEMENTS

EUMETSAT provided the Meteosat-8 SEVIRI images and the SEVIRI Preprocessing Toolbox. We also would like to thank Jean-Marie Bettems, Igor Giunta and Hans Peter Roesli of MeteoSwiss for their input.

7. REFERENCES

ALLEN, R. C. Jr., DURKEE, P. A. and WASH. C. H., (1990) Snow/cloud discrimination with multispectral satellie measurements. Journal of Applied Meteorology, 29, pp 994-1004

BAUM, B. A. and TREPTE, Q., (1999) A grouped threshold approach for scene identification in AVHRR imagery. Journal of Atmospheric and Oceanic Technology, 16, pp 793-800

DOZIER, J., (1989) Spectral signature of alpine snow cover from the Landsat Thematic Mapper. Remote Sensing Environment, 28, pp 9-22

EBERT, E. A., (1987) A pattern recognition technique for distinguishing surface and cloud types in the polar regions. Journal of Climate and Applied Meteorology, 26, pp 1412-1427

GESELL, G., (1989) An algorithm for snow and ice detection using AVHRR data. An extension to the APOLLO software package. International Journal of Remote Sensing, 10, 4 and 5, pp 897-905

HALL, D. K., RIGGS, G. A. and SALOMONSON, V. V., (1995) Development of methods for mapping global snow cover using moderate resolution imaging spectroradiometer data. Remote Sensing Environment, 54, pp 127-140

HALL, D. K., RIGGS, G. A., SALOMONSON, V. V., DIGIROLAMO, N. E. and BAYR, K. J., (2002) MODIS snow-cover products. Remote Sensing Environment, 83, pp 181-194

López Cotín, L. F., (2005) User Manual for the PGE01-02-03 of the SAFNWC / MSG: Scientific part. EUMETSAT SAFNWC / Météo-France, document SAF/NWC/IOP/MFL/SCI/SUM/01, Issue 1.2

LOGAR, A. M., LLOYD, D. E., CORWIN, E. M., PENALOZA, M. A., FEIND, R. E., BERENDES, T. A., KUO, K.-S. and WELCH, R. M., (1998) The ASTER Polar Cloud Mask. IEEE Transactions on Geosciences and Remote Sensing, 36, 4, pp 1302-1312

RIGGS, G. and HALL, D. K., (2002) Reduction of cloud obscuration in the MODIS snow data product. In: Proceedings of the 59th Eastern snow conference (Stowe, Vermont)

ROMANOV, P., GUTMAN, G. and CSISZAR, I., (2000) Automated monitoring of snow cover over North America with multispectral satellite data. Journal of Applied Meteorology, 39, pp 1866-1880

ROMANOV, P., TARPLEY, D., GUTMAN, G. and CARROLL, T., (2003) Mapping and monitoring of the snow cover fraction over North America. Journal of Geophysical Research, 108, D16, art. no. 8619

WELCH, R. M., BERENDES, D., BERENDES, T. A., KUO, K.-S. and LOGAR, A. M., (1999) The ASTER polar cloud mask algorithm theoretical basis document. NASA EOS ASTER, ATBD-AST-13

WU, R., WEINMAN, J. A. and CHIN, R. T., (1985) Determination of rainfall rates from GOES satellite images by a pattern recognition technique. Journal of Atmospheric and Oceanic Technology, 2, 3, pp 314-330

SOIL MOISTURE FROM THERMAL INFRARED SATELLITE DATA: ENVISAGED SYNERGIES WITH METOP ASCAT DATA

W. Wagner and C. Künzer

Institute of Photogrammetry and Remote Sensing
Vienna University of Technology
Gusshausstr. 27-29, A-1090 Wien, Austria

ABSTRACT

Within EUMETSAT's network of Satellite Application Facilities (SAFs) different approaches for developing soil moisture products have been followed. Within the SAF for Land Surface Analysis (Land SAF) a thermal approach based on METEOSAT and MSG data has been followed for deriving soil moisture and evapotranspiration, while the SAF on Support to Operational Hydrology and Water Management (H-SAF) pursues the development of microwave derived soil moisture products based on METOP ASCAT data. So far, these developments have gone on largely independently but many potential synergies between the two approaches exist. In this paper we make a short review of thermal methods for soil moisture retrieval and discuss potential benefits of merging thermal and microwave data for deriving soil moisture. The strongest argument for working towards a synergistic thermal-microwave product is the envisaged capability of such a synergistic product to bridge and connect the two scales existing in soil moisture remote sensing – the local scale dominated by vegetation-, topography- and soil influences and the global scale, where atmospheric forcing influences large scale soil moisture patterns. Also, modelling the profile soil moisture content based on the remotely sensed surface data would most likely benefit because moisture and temperature diffusion in the profile are related. Eventually, also the Land SAF evapotranspiration product would benefit from such an advanced soil moisture product.

1. THERMAL PARAMETERS AS A KEY FOR SOIL MOISTURE DERIVATION

A large variety of approaches for the retrieval of soil moisture from satellite data exist (Engman and Chauhan 1995, Wagner et al. 2006). The majority of these approaches rely on microwave sensors, encompassing microwave radiometers and scatterometers for regional to global applications, and Synthetic Aperture Radars (SARs) for local scale applications. The first satellite dedicated for monitoring soil moisture over land is the Soil Moisture and Ocean Salinity (SMOS) mission of the European Space Agency (ESA) that is scheduled for launch in 2007. It is a passive radiometer operated at a wavelength of about 21 cm (L-band). Another sensor suited for soil moisture monitoring is the Advanced Scatterometer (ASCAT) on-board of a series of three METOP satellites operated by the European Organization for the Exploitation of Meteorological Satellites (EUMETSAT). The first METOP satellite will be launched in summer 2006. All three satellites are foreseen to cover a period of 14 years. The ASCAT is operated at a shorter wavelength (5.6 cm, C-band) compared to SMOS, reducing its sensitivity to soil moisture over vegetated areas somewhat. However, ASCAT is expected to achieve a high radiometric accuracy and a high temporal stability of the signal comparable to its successor, the ERS-1/2 scatterometer. Based on the latter sensor the first remotely-sensed, global, multi-year soil moisture dataset has been derived (Wagner et al. 2003). Currently work is underway at the Vienna University of Technology to develop software for near-real-time processing of 25 km ASCAT surface soil moisture products in orbit geometry. It is planned to implement the software at EUMETSAT's central processing facility, which will allow delivering global surface soil moisture data to meteorological services and other users within 135 minutes after sensing via EUMETCast. For Europe, a dedicated ASCAT soil moisture product for hydrologic users is currently under development within EUMETSAT's Satellite Application Facility (SAF) on Support to Operational Hydrology and Water Management (H-SAF). More information about the ASCAT soil moisture products can be found at http://www.ipf.tuwien.ac.at/radar/.

A major advantage of ASCAT and SMOS are their near-global coverages and their ability to sense the land surface independent of cloud cover and daytime. Thus, ASCAT and SMOS guarantee frequent temporal coverage. Also, both sensors provide a rather direct measure of the soil moisture content due to the pronounced dependency of microwave emission and backscatter on the soil dielectric properties, and hence on soil moisture. However, their spatial resolution is only in the order of tens of kilometres (25-50 km), which will probably be a severe limitation of the usability of these data in many applications. Other microwave derived products with higher spatial resolution such as Envisat ASAR derived soil moisture at < 1km do often not allow for sufficient timely and areal coverage. To overcome some of the limitations of "stand-alone" microwave systems, it seems attractive to use synergistic information from other remote sensing systems. In this paper we want to address how thermal infrared (TIR) remote sensing data – as e.g. provided by Meteosat Second Generation (MSG) – might be utilized in synergy to METOP ASCAT to provide advanced soil moisture products. To this end we make a short review of the state of the art in soil moisture retrieval from thermal data and discuss synergies with respect to thematic content, spatial resolution, temporal sampling, accuracy or data availability.

2. THERMAL PARAMETERS AS A KEY FOR SOIL MOISTURE DERIVATION

Thermal remote sensing data is usually acquired in the 8.0-14.0 µm TIR wavelength domain. A widely applicable direct link between temperature data and soil moisture does not exist (Jackson et al. 1997). Also soil moisture does not directly enter the energy balance equation of the land

surface. However, the water content of a soil strongly influences the evapotranspiration term of the equation as well as the specific heat capacity and emissivity in the same. The thermal expression of a soil is thus altered depending on its moisture content and thermal physical parameters can support the indirect retrieval of information on soil moisture conditions. Many authors have followed this direction of TIR based soil moisture estimation utilising a large variety of data from sensors such as HCMM, TIROS-N, NOAA-AVHRR, GOES, Meteosat and Landsat amongst others (Carlson 1986, Carlson et al. 1984, Jones et al. 1998, McNider et al. 1994, Portman et al. 2003, Price, 1998, Rosema et al. 2001, Shih and Jordan 1993, van den Hurk 2001, Verstraeten et al. 2006, Wetzel and Woodward 1987). Approaches range from simple indices to the assimilation in soil-vegetation-atmosphere transfer (SVAT) models. Such models are often highly complex and need a large number of input variables to yield sufficient results. Boundary conditions or parameters are often adjusted to match observed variables. Hence, the obtained results strongly depend on the choice of the SVAT model, the chosen input parameters and the accuracy of the latter. For example, Portman et al. (2003) modified the TESSEL model and adjusted model soil moisture so that a modelled surface temperature rise matched observed in-situ temperature increases. However, large scale or even globally applicable approaches with high temporal resolution offering operational readiness have only been implemented in rare cases. Rosema et al. (2001) have developed several products within the Energy and Water Balance Monitoring System (EWBMS). Amongst others, a soil moisture index is derived from diurnal Meteosat data calculating a ratio of actual evapotranspiration and potential evapotranspiration, expressed in %. The EWBMS has been implemented over Europe, Africa and parts of Asia. Another promising concept was recently presented by Verstraeten et al. (2006), which combines thermal inertia retrieval as introduced by numerous authors as early as the 1970s (Rose 1968, Idso et al. 1975, Schmugge et al. 1978, Sabins 1996), with the principles of the scatterometer derived soil moisture index derivation as developed and implemented by Wagner et al. (1999).

Of great potential for TIR based soil moisture retrieval is the concept of thermal inertia of an object, P (cal/cm²/sec$^{-0.5}$/ °C), which is defined as the resistance of an object against its heating for 1°C, depending on three measures. Firstly, the specific warmth, c, which is the energy needed to rise the temperature of a material for 1°C (heat capacity C) per mass unit of the substance (m), secondly the density of a material, p – the main determining factor – and thirdly the thermal conductivity, k, of an object. Hence, $P = (c \cdot k \cdot p)^{0.5}$. Variations of P affect diurnal temperature difference ΔT, defined as the difference between the maximum and minimum temperature occurring during a diurnal solar cycle (Kahle et al. 1976). Low thermal inertias indicate low resistance to temperature changes, resulting in a high ΔT. The opposite applies for materials with a high thermal inertia, e.g. water. Hence, ΔT decreases with increasing soil moisture. While remote sensing does not allow for the direct derivation of P (c, p and k can only be measured in-situ) the concept still allows to exploit the impact of soil moisture upon T and ΔT. Maximum and minimum radiant temperature can be measured from thermal daytime and nighttime remote sensing images. ΔT is calculated subtracting the nighttime temperature from the daytime temperature for corresponding ground resolution cells. Already Idso et al. (1975) and Schmugge et al. (1978) investigated the potential of ΔT for soil moisture retrieval and found the data helpful to infer moisture in the 0-4cm horizon. Later, the relationship of low ΔT for materials with a high P and vice versa, was extended to calculate the so called Apparent Thermal Inertia, ATI. It is defined as $ATI=(1-A)/\Delta T$, where A is the albedo of the pixel in the visible band. The albedo is included to compensate for the effect that dark materials with low albedo absorb more sunlight than light materials with a high albedo. Hence, by including the term 1-A, the effect that a dark material typically has a higher ΔT than an otherwise identical light material is somewhat compensated. ATI, however, cannot compensate for relief induced variations in ΔT. In an area of uniform material shadowed areas have a lower radiant temperature during the day and hence a lower ΔT than the exact same material exposed on a sunlit slope. Here, topographic data and solar elevation and

azimuth information can be employed to overcome relief induced variation of ΔT. Depending on the resolution of the datasets and the scale of an envisaged product this might not play a crucial role though.

3. RECENT CASE STUDIES

The concept of ATI has already been applied in Sabins (1996) and by Cracknell and Xue (1996) and was recently employed by Verstraeten et al. (2006) comparing ATI derived soil moisture from Meteosat data with in-situ data and ERS-Scat derived soil water index (SWI) data. Since ATI represents the temporal and spatial variability of soil- and canopy moisture the highest and lowest ATI values in an ATI time series for a specific pixel can represent the residual and saturated soil moisture. Verstraeten et al. (2006) thus derive a change detection based soil moisture saturation index (SMSI) according to the quotient $SMSI = (ATI_t - ATI_{min})/ATI_{max} - ATI_{min})$, which is modified further to retrieve soil moisture content (SMC). Additionally, they employ a filtering approach developed by Wagner et al. (1999) which estimates the status of soil profile moisture content (SMC) based on time series of the surface soil moisture content. Correlation coefficients between SMC results and EUROFLUX site in-situ data as well as ERS scatterometer derived SWI are satisfactory. Verstraeten et al. (2006) discuss that the errors retrieved from this TIR based approach are in the same order of magnitude as those reported for microwave derived soil moisture products. We consider the presented approach as highly capable for operational retrieval of soil moisture from TIR data and suggest to initiate case studies for further in depth evaluation.

The positive results from a TIR based approach are also supported by results of Naeimi et al. (2006). They compared four satellite soil moisture time series data sets derived with four different approaches from three different sensors. Correlation coefficients between the TDR probe in-situ data and ERS Scatterometer derived soil moisture, two AMSR-E derived soil moisture products and the Meteosat derived TIR based soil moisture index presented by Rosema (2001) range from 0.64 for the ERS-Scat derived product to 0.83 for an AMSR-E product developed by the Vrije University of Amsterdam. The Meteosat product yields a satisfactory R of 0.65.

In another study, van den Hurk (2001) compared three different satellite algorithms for TIR based soil moisture estimation, namely the Surface Energy Balance Algorithm for Land, SEBAL, the Surface Energy Balance Index, SEBI and the “heating rate method” proposed by Wetzel and Woodward (1986). While SEBAL and SEBI compute pixelwise solutions for all components of the surface energy balance equation and derive soil moisture via the latent heat and evaporation parameters, the heating rate method postulates that ΔT depends on available radiation, surface type and moisture availability. Via a set of equations the soil moisture content is derived by forcing the model heating rate to match the satellite derived heating rate. Similarly, Jones et al. (1997) include satellite observed TIR heating rates into a mesoscale atmospheric model to retrieve soil moisture. Although van den Hurk (2001) favors the heating rate methods due to its straightforwardness, none of the methods have been used operationally in NWP applications.

Several other approaches based on relatively high resolution data, e.g. Landsat multi-spectral and thermal imagery, exist (Shih and Jordan, 1993). However, since we consider these approaches as not applicable for sufficient spatial or temporal coverage we do not discuss them further. Nevertheless, it should be kept in mind that TIR approaches can be pursued with any sensor data offering diurnal coverage. For locally intended case studies and hydrologists working on specific catchments such data might do sufficiently.

4. SYNERGY OF MICROWAVE AND THERMAL DATA FOR NEW PRODUCTS

There are some shortcomings of the TIR based soil moisture retrieval approaches. Firstly, surface information cannot be retrieved during cloud cover conditions, an option, which is unique to microwave frequencies below 10 GHz. Secondly, soil moisture can only be retrieved indirectly by analysing its effect on surface temperature and other surface variables. Furthermore, some authors (Jackson et al. 1997) discuss that TIR based soil moisture retrieval works for rather dry conditions only. This is due to the fact that land surface temperature (LST) is controlled by evaporation as long as the soil is relatively wet. Only as it dries it is controlled by thermal inertia. In addition, the importance of the P effect decreases as vegetation cover increases because of radiation shielding effects and increased evapotranspiration from leaves. As a last point, the effect of wind on the surface temperature should be mentioned. While, in principle, the physical mechanisms are well understood, in practice it is difficult to account for wind due to the lack of wind observations.

Nevertheless, advantages of the simultaneous retrieval of soil moisture from thermal and microwave data are at hand. Diurnal thermal data is available on a daily basis from Meteosat at a nadir resolution of 5km, from MSG's Seviri instrument at 3 km, from NOAA-AVHRR at 1.1 km and from MODIS at 1km nadir resolution respectively. Soil moisture products derived via diurnal thermal inertia approaches could thus convince with much higher spatial detail than daily available 25 km ASCAT products. The thermal approach could be especially beneficial in areas of low cloud cover. Weekly products interpolated for cloud gaps could deliver additional data for mid-latitude regions. The LST of a pixel is mainly dependant on the object's albedo, its thermal inertia and outer conditions such as relief and wind. The roughness component, which is influencing microwave derived products is negligible in the 8-14 µm part of the spectrum. Provided that the albedo component can be corrected through a visible band as incorporated in the ATI approach, in even terrain the thermal signal is then mainly governed by the material's composition itself. For natural environments the LST is then mainly a function of material- (surface-) moisture.

From an user perspective the strongest argument for working towards a synergistic thermal-microwave product is the envisaged capability of such a synergistic product to bridge and connect the two scales existing in soil moisture remote sensing – the local scale dominated by vegetation-, topography- and soil influences and the global scale, where atmospheric forcing influences large scale soil moisture patterns (Etin et al., 2000). This connection widens the user group from globally or country-wide operating users to users interested in the regional scale. Especially in highly complex terrain TIR data has an advantage to actively sensed scatterometer data, which are strongly influenced in their backscattering signal by difficult terrain (Parajka et al. 2006).

Further refinements can be expected for the modelling of the infiltration process and thus the derivation of the profile soil moisture content. Here accuracy is thought to improve since moisture and temperature diffusion in the profile are related (Entekhabi et al. 1994). Thus, research is needed to fuse profile soil moisture estimation approaches as presented from the microwave and the thermal domain.

Besides technical and scientific arguments it is also important that users – who are generally not remote sensing experts – comprehend the information content of a product. In this respect, a disadvantage of microwave technologies is that a good physical understanding is in general necessary to understand the benefits and shortcomings of microwave products. On the other hand, thermal imagery is more widely accepted, since temperature images can be more readily interpreted. Therefore, a soil moisture product derived from a thermal dataset might find a greater

overall acceptance in the geo-science community. Also, data from NOAA-AVHRR, METEOSAT, MSG or MODIS is more widely used and users might be less sceptical to products derived thereof.

In brief, the benefits of a synergistic soil moisture product based on TIR and ASCAT data might be as follows:

- Higher spatial and temporal resolution, increase in detail
- Bridging the gap between local and global scale
- Offering cross validation and comparison options for time series and neighbour disciplines
- Improved modelling of moisture and temperature diffusion over the soil profile
- Acceptance by (new) user community expected

Hence, we propose to further investigate the possibilities of merging thermal products – as provided by EUMETSAT's SAF on Land Surface Analysis (Land-SAF) – with ASCAT soil moisture products provided by EUMESAT and the H-SAF. Especially ATI based products seem very appealing with respect to their simplicity.

5. BIBLIOGRAPHIC REFERENCES

CALVET, J.-C., NOILHAN, J. and BESSEMOULIN, P. (1998) Retrieving the root-zone soil moisture from surface soil moisture or temperature estimates: a feasibility study based on field measurements. J. Appl. Meteor., 37(4), pp. 371-386.

CARLSON, T. N. (1986) Regional-Scale Estimates of Surface Moisture Availability and Thermal Inertia Using Remote Thermal Measurements. Remote Sensing Reviews, 1, pp. 197-247.

CARLSON, T. N., ROSE, F. G. and E. M PERRY (1984) Regional-Scale Estimates of Surface Moisture Availability from GOES Infrared Satellite Measurements. Agronomy Journal, 76, pp. 972-979.

CRACKNELL, A.P. and Y. XUE (1996) Thermal inertia determination from space – a tutorial review, International Journal of Remote Sensing, 17, pp. 431-461.

ENGMAN, E. T. and CHAUHAN, N. (1995) Status of microwave soil moisture measurements with remote sensing. Remote Sens. Environ., 51, pp. 189-198.

ENTEKHABI, D., NAKAMURA, H, and NJOKU, E.G. (1994) Solving the inverse problem for soil moisture and temperature profiles by sequential assimilation of multifrequency remotely sensed observations. IEEE Transactions on Geoscience and Remote Sensing, 32(2), pp. 438-448

ENTIN, J.K., ROBOCK, A., VINNIKOV, K.Y., HOLLINGER, S.E., LIU, S., and NAMKHAI, A. (2000). Temporal and spatial scales of observed soil moisture variations in the extratropics. J. Geophys. Res., 105, pp. 11865-11877.

IDSO, S. B., SCHMUGGE, T. J., JACKSON, R. D. and R. J. REGINATO (1975) The utility of surface temperature measurements for the remote sensing of surface water soil status, J. Geophysical Res., 80, pp. 3044-3049.

JACKSON, T. J., O'NEILL, P. E. and C. T SWIFT (1997) Passive Microwave Observation of Diurnal Surface Soil Moisture. IEEE Transaction on Geoscience and Remote Sensing, 35, 1210-1222.

JONES, A. S., GUCH, I. C., and VONDER HAAR, Th. H. (1998) Data assimilation of satellite-derived heating rates as proxy surface wetness data into a regional atmospheric mesoscale model, Part II: A case study. Mon. Wea. Rev., 126, pp. 646-667.

KAHLE, A.B., GILLESPIE, A.R. and A.F.H. GOETZ (1976) Thermal Inertia Imaging: a new geological mapping tool. Geophysical Research Letters, 3, pp. 26-28.

MCNIDER, R. T., SONG, A. J., CASEY, D. M., WETZEL, P. J., CROSSON, W. L., and RABIN, R. M., (1994) Toward a dynamic-thermodynamic assimilation of satellite surface temperature in numerical atmospheric models. Mon. Wea. Rev., 122, pp. 2784-2803.

NAEIMI, V., WAGNER, W., SCIPAL, K., DE JEU, R. and J. MARTÍNEZ-FERNÁNDEZ (2006) Soil Moisture from Operational Meteorological Satellites. Hydrogeology Journal, submitted and accepted.

PARAJKA, J., NAEIMI, V., BLÖSCHL, G., WAGNER, W., MERZ, R. and K. SCIPAL (2006) Assimilating scatterometer soil moisture data into conceptual hydrologic models at the regional scale. Hydrol. Earth Syst, Sci., 10, pp. 353-368.

PORTMANN, F., W. WAGNER, and K. SCIPAL, (2003) Evaluation of early morning heating rate derived soil moisture in Southern Europe. The 2003 Eumetsat Meteorological Satellite Conference, Weimar, Germany, 29 September - 3 October 2003.

PRICE, J.C. (1980) The Potential of Remotely Sensed Thermal Infrared Data to Infer Surface Soil Moisture and Evaporation. Water Resources Research, 16, 4, 787-795.

ROSE, C. W. (1968) Water transport in soil with a daily temperature wave – theory and experiments. Australian J. Soil Res., 6, pp. 31-44.

ROSEMA, A., and COAUTHORS, (2001) European Energy and Water Balance Monitoring System (EWBMS): Final Report April 2001. The European Community Framework Programme (Theme3, Area 3.1.2), Contract number: ENV4-CT97-0478, 147 pp.

SABINS, F.F. (1996) Remote Sensing. 3rd edition, New York, USA, 450 pp.

SCHMUGGE, T., BLANCHARD, B., ANDERSON, A and J. WANG (1978) Soil moisture sensing with aircraft observations of the diurnal range of surface temperature, Water Resources Bull., 14, pp. 169-178.

SHIH, S. F. and J. D. JORDAN (1993) Use of Landsat Thermal-IR Data and GIS in Soil Moisture Assessment. Journal of Irrigation and Drainage Engineering, 119(5), pp. 868-879.

VAN DEN HURK, B., (2001) Energy balance based surface flux estimation from satellite data, and its application for surface soil moisture estimation. Meteorol. Atmos. Phys., 76, pp. 43-52.

VERSTRAETEN, W. W., VEROUSTRAETE, F., VAN DER SANDE, C. J. GROOTAERS, I. and J. FEYEN (2006) Soil moisture retrieval using thermal inertia, determined with visible and thermal spaceborne data, validated for European forests. Remote Sens. Environ., 101(3), pp. 299-314.

WAGNER, W., K. SCIPAL, C. PATHE, D. GERTEN, W. LUCHT, and B. RUDOLF (2003) Evaluation of the agreement between the first global remotely sensed soil moisture data with

model and precipitation data, Journal of Geophysical Research D: Atmospheres, 108(19), ACL 9-1 – pp. 9-15.

WAGNER, W., PAMPLONI, P., BLÖSCHL, G., CALVET, J.-C., BIZZARRO, WIGNERON, J.-P. and Y. KERR (2006) Operational Readiness of Microwave Remote Sensing of Soil Moisture for Hydrologic Applications. Submitted to Nordic Hydrology

WAGNER, W., LEMOINE, G., and ROTT, H. (1999) A method for estimating soil moisture from ERS Scatterometer and soil data. Remote Sens. Environ., 70, pp. 191-207.

WETZEL P. J., and R. H. WOODWARD (1987) Soil moisture estimation using GOES-VISSR Infrared data: A case study with a simple statistical method. J. Climate Applied Meteor., 26, pp. 107-117.

ACTUAL EVAPORATION, SENSIBLE HEAT FLUX AND REFERENCE CROP EVAPOTRANSPIRATION AS POTENTIAL NEW LAND SAF PRODUCTS

Henk de Bruin

Wageningen Universiteit

WAGENINGEN UNIVERSITEIT

ACTUAL EVAPORATION, SENSIBLE HEAT FLUX and CROP EVAPOTRANSPIRATION

As potential LANDSAF products

Henk de Bruin, Oscar Hartogensis and Arnold Moene

WAGENINGEN UNIVERSITEIT

Our background

- **Atmospheric Turbulence and micrometeorology**
  - **Boundary Layer Meteorology**
- **Land Surface Processes and its parametrization**
  - **No real MSG-LANDSAF background**

IRRIMED *LANDSAF WORKSHOP, 8-10 March, LISBON* WAGENINGEN UR

WAGENINGEN UNIVERSITEIT
WAGENINGEN UR

Topics

Part 1. Turbulent Heat Fluxes on kilomter scale and Scintillometry , final goal mapping fluxes

Part 2. Radiantion based estimates of actual evaporation in the Tropics and of Crop Reference Evapotranspiration, for agricultural applications

WAGENINGEN UNIVERSITEIT
WAGENINGEN UR

Surface Heterogeneity on km scale: LITFASS

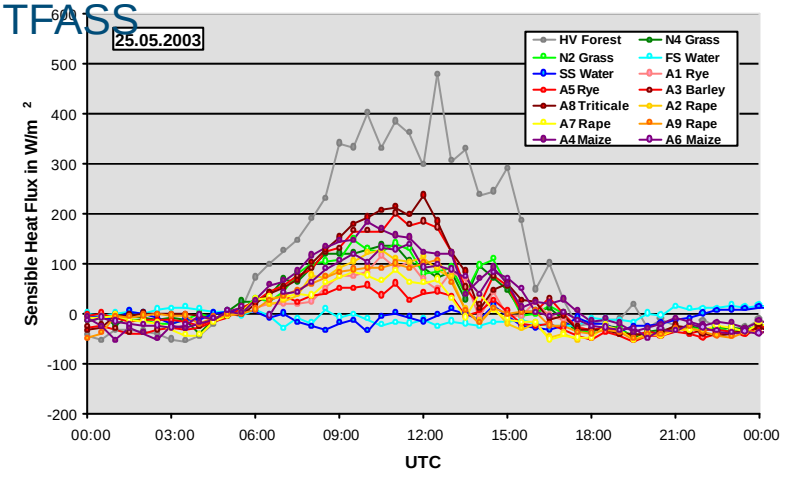

Fluxes over Different Surfaces within a grid of 15 x 15 km

WAGENINGEN UNIVERSITEIT

Scale issue

Validation of any method to derive fluxes from MSG requires an indepenent observation method that works over heterogeneous terrain on the MSG spatial scale.

Points to make:

- **Scintillometry is a suitable technique for validation of any LANDSAF flux product**
- **Scintillometer-MSG-ECMWF system is worthwhile to develop.**

WAGENINGEN UNIVERSITEIT

Scintillometer

D =aperture transmitter

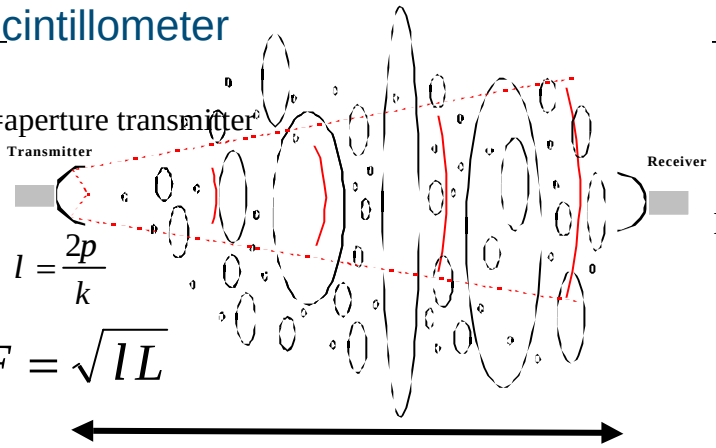

D =aperture receiver

$$l = \frac{2p}{k}$$

$$F = \sqrt{lL}$$

Path length (L) = 1 – 10 km

Remote-sensing technique at the ground (geostationary)

IRRIMED LANDSAF WORKSHOP, 8-10 March, LISBON WAGENINGEN UR

WAGENINGEN UNIVERSITEIT

What is measured?

- **the *variance* of the logarithm of the light amplitude received by the detector.**

$$s_c^2 = 0.892 C_n^2 D^{-\frac{7}{3}} L^3 \qquad D > F$$

$$s_c^2 = 0.124 C_n^2 k^{\frac{7}{6}} L^{\frac{11}{6}} \qquad F > D$$

Large Apeterure Scintillometer
l about 1 micron

LAS

Radio Wave Scintillometer
l about 1 cm or 30GHz

RWS

WAGENINGEN UNIVERSITEIT

Simplified Picture

LAS gives C_T^2 and RWS gives C_Q^2 :

Once C_T^2 and C_Q^2 are known, H and L_vE can be estimated applying the Monin-Obukhov Similarity Theory

During daytime free convection scaling dominates!!!!

$$H \cong z\left(\frac{g}{T}\right)^{\frac{1}{2}} \left(C_T^2\right)^{\frac{3}{4}}; \qquad E \cong z\left(\frac{g}{T}\right)^{\frac{1}{2}} \left(C_T^2\right)^{\frac{1}{4}} \left(C_Q^2\right)^{\frac{1}{2}}$$

Fluxes are on scale of half the path length, so MSG pixel

WAGENINGEN UNIVERSITEIT

Radio Wave Scintillometer

WAGENINGEN UNIVERSITEIT

Toulouse 2005- XLAS

IRRIMED LANDSAF WORKSHOP, 8-10 March, LISBON WAGENINGEN UR

WAGENINGEN UNIVERSITEIT

Toulouse 2005- present landscape

WAGENINGEN UNIVERSITEIT

Flevoland Experiment 1998 (2 km)

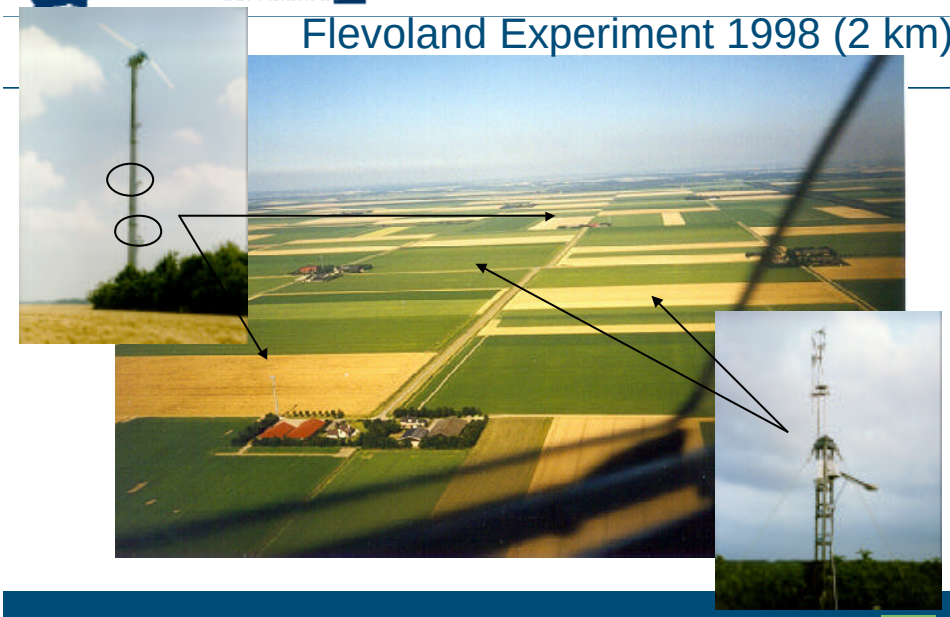

IRRIMED LANDSAF WORKSHOP, 8-10 March, LISBON WAGENINGEN UR

WAGENINGEN UNIVERSITEIT
WAGENINGEN UR

Flevoland: Latent heat flux from LAS

= Simple estimate ***net radiation*** and ***soil heat flux*** minus H_{LAS}

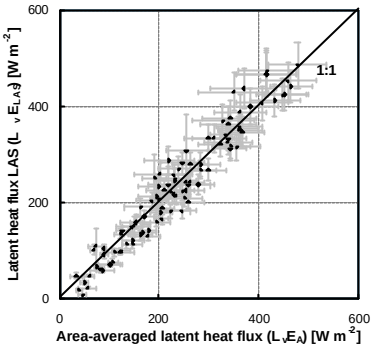

WAGENINGEN UNIVERSITEIT
WAGENINGEN UR

LITFASS, Lindenberg, Germany

IRRIMED LANDSAF WORKSHOP, 8-10 March, LISBON WAGENINGEN UR

WAGENINGEN UNIVERSITEIT
WAGENINGEN UR

LITFASS-2003: The measurement strategy

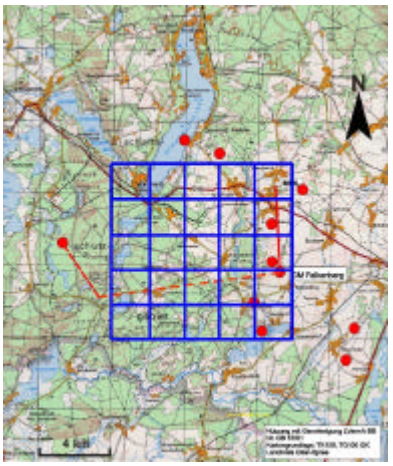

WAGENINGEN UNIVERSITEIT
WAGENINGEN UR

LITFASS-2003: Fluxes over Different Surfaces

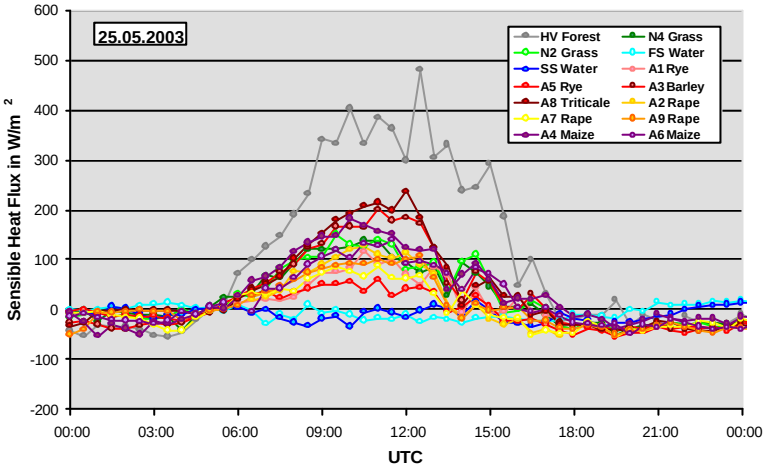

WAGENINGEN UNIVERSITEIT

LITFASS-2003: Area-averaged Fluxes (I)

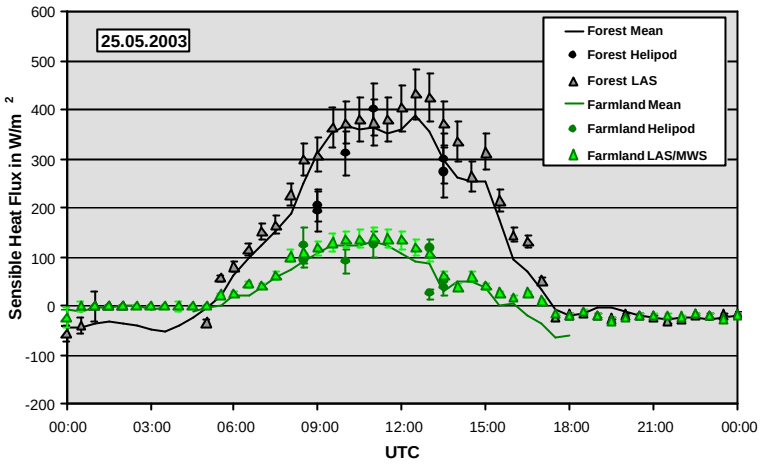

WAGENINGEN UNIVERSITEIT

LITFASS-2003: Area-averaged Fluxes (I)

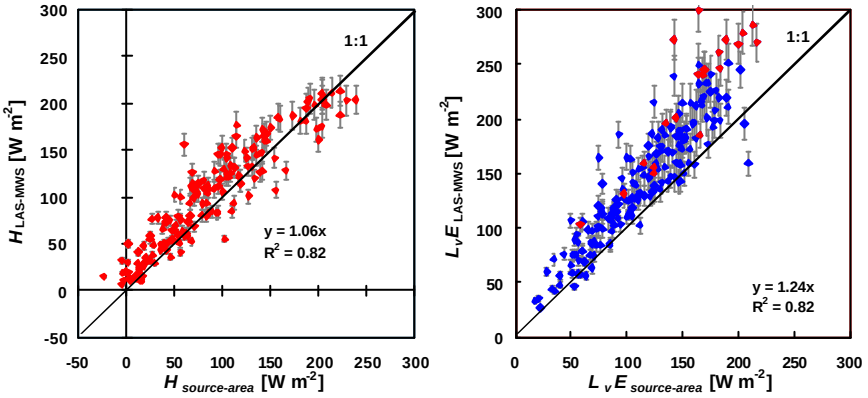

WAGENINGEN UNIVERSITEIT

Proposal for use of scintillometry in LANDSAF

Validation phase

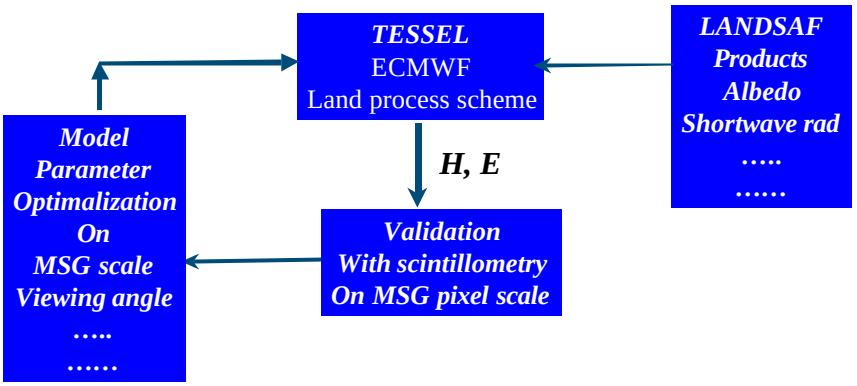

WAGENINGEN UNIVERSITEIT

Proposal for use of scintillometry in LANDSAF

Operational phase

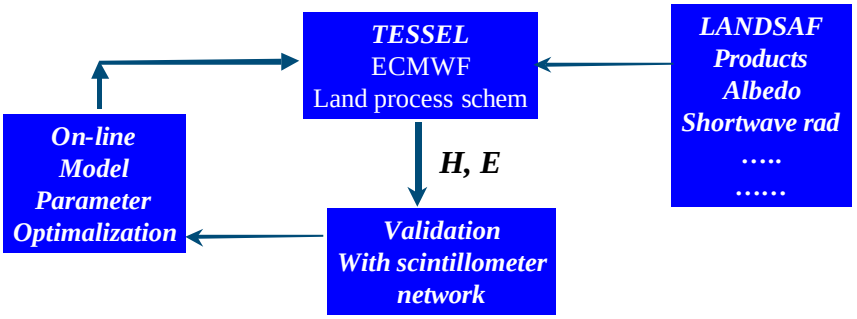

WAGENINGEN UNIVERSITEIT

Proposal for use of scintillometry in GMES

Drought monitoring

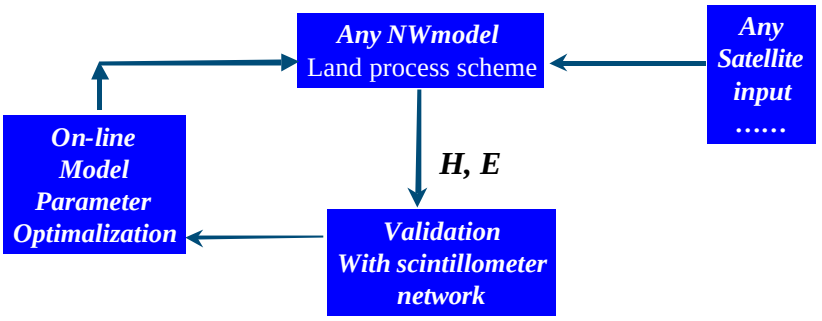

WAGENINGEN UNIVERSITEIT

Part 2 Radiation based Evaporation estimates

a. Actual evapotranspiration

Application: Ghana, deep rooting bushes and rain-triggered grass

$$E_{opt} = k_c E_{ref}$$

$$E_{ref} = 0.65 \frac{s}{s+g} R_s$$

$$E_{act} = VF * E_{opt}$$

- k_c = crop factor
- R_s = incoming solar radiation in W m^{-2}
- s =slope of water vapor pressure at constant temperature
- ? is the psychrometric constant
- VF = vegetation fraction

IRRIMED LANDSAF WORKSHOP, 8-10 March, LISBON WAGENINGEN UR

WAGENINGEN UNIVERSITEIT

Final algorithm

$$E_{act} = VF * E_{opt} + (1 - VF) E_{soil} + E_{\text{int}}$$

Application: Ghana, deep rooting bushes and rain-triggered grass

WAGENINGEN UNIVERSITEIT

Baseline method with other input

- Global radiation DLR (Meteosat) ? global radiation from MSG (Land-SAF)
- Vegetation fraction MODIS (EVI) ? vegetation fraction from MSG (Land-SAF)
- Near surface temperature DLR (Meteosat) ? atmospheric model data
- Land cover (USGS) ? land cover used by Land-SAF / DLR for GLOWA-Volta

IRRIMED LANDSAF WORKSHOP, 8-10 March, LISBON WAGENINGEN UR

WAGENINGEN UNIVERSITEIT

Actual ET in Ghana 15 November 2002 Validated with scintillometry

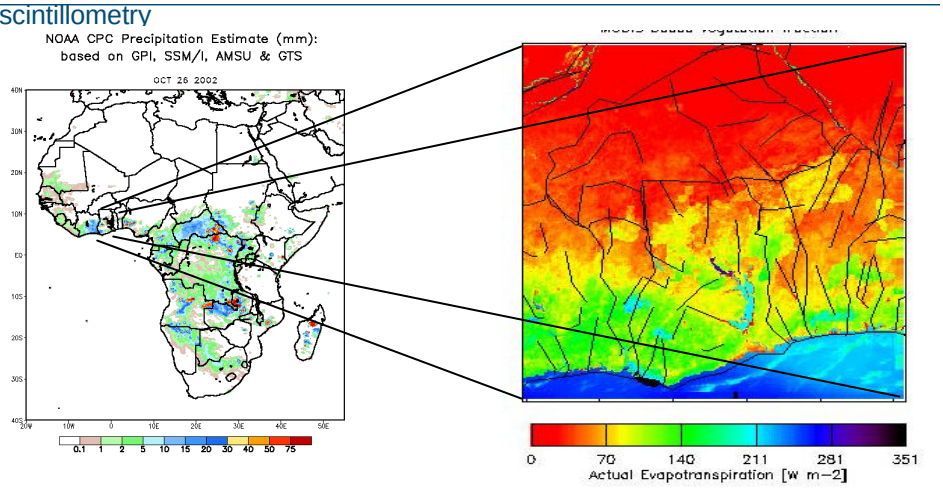

WAGENINGEN UNIVERSITEIT

Crop Reference Evapotranspiration (FAO)

$$E_{opt} = k_c E_{ref}$$

Proposal to use $$E_{ref} = 0.65 \frac{s}{s+g} R_s$$

- k_c = crop factor
- R_s = incoming solar radiation in W m^{-2}
- s =slope of water vapor pressure at constant temperature
- ? is the psychrometric constant

IRRIMED LANDSAF WORKSHOP, 8-10 March, LISBON WAGENINGEN UR

WAGENINGEN UNIVERSITEIT

Crop Reference Evapotranspiration (FAO)

Reference crop refers to short well-watered grass growing in very large fields (no advection)

In Spain there are a number of FAO lysimeter station covered and surrounded with well-watered grass

e.g. at Zaragoza

WAGENINGEN UNIVERSITEIT

ET_{ref} from MSG (DEMETER and PLEIADeS)

Basic thought:

- ET_{ref} is defined for very large fields, then advection is absent and ET_{ref} is expected to be determined by 'available energy source, i.e. Radiation.
- The latter can be derived from MSG

IRRIMED LANDSAF WORKSHOP, 8-10 March, LISBON WAGENINGEN UR

WAGENINGEN UNIVERSITEIT

Analyses Zaragoza data

1 mm/day = 29 W/m^2

W/m^2

ET$_{ref}$ FAO

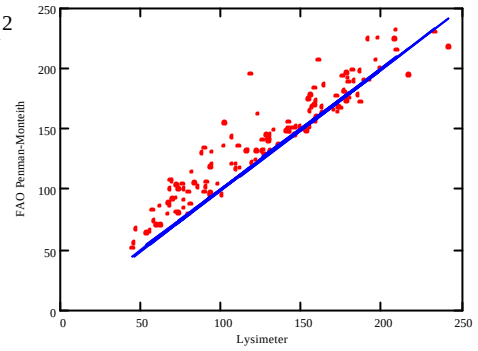

WAGENINGEN UNIVERSITEIT

Comparison with Makkink (U< 3 m/s)

Makkink

$$E_{ref} = 0.65 \frac{s}{s+g} R_s$$

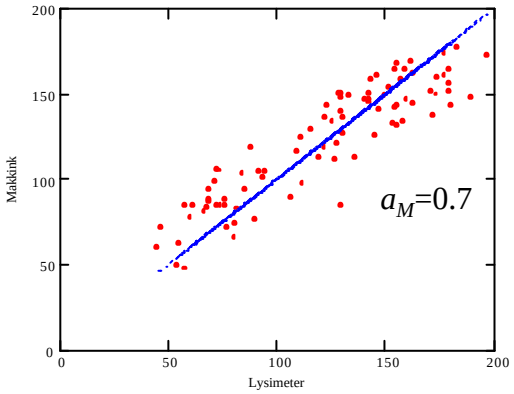

Lysimeter

WAGENINGEN UNIVERSITEIT

Comp. with Priestley-Taylor

Low wind speed: u < 3 m/s

Priestley-Taylor

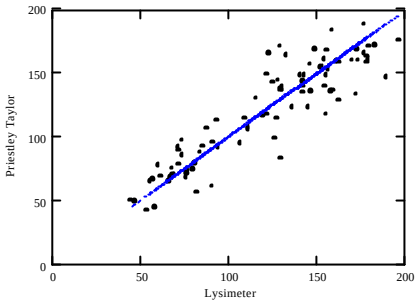

a_{PT}=1.3

Lysimeter

WAGENINGEN UNIVERSITEIT

Conclusions

- The scintillometer method is a suitable observation technique to validate any LANDSAF ET product
- A combined Scintillometer-MSG-TESSEL(ECMFW) approach to map surface fluxes is worthwhile to develop
- The radiation based approximation of ET_{act} using MSG derived Downwelling Short-wave in tropical regions (deep rooting shrubs/trees and rain-responding grases) is a promising approach
- The radiation based approximation of ET_{ref} using MSG derived Downwelling Short-wave radiation is suitable for operational applications in agricultural practice (after systematic testing)

IRRIMED LANDSAF WORKSHOP, 8-10 March, LISBON WAGENINGEN UR

WAGENINGEN UNIVERSITEIT

Examples

Date:

11/15/2002

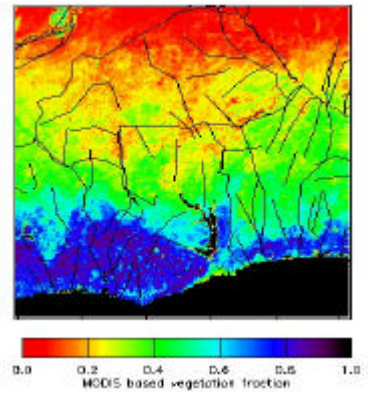

WAGENINGEN UNIVERSITEIT

Examples

Issues for LandSaf Workshop Working Groups

Proposal for developing and testing:

1. ET_{ref} -MSG products
2. ET_{actual}-MSG following our work in Ghana
3. Validating MSG-ET products with scintilloemeters
4. (long term objective) Sintillometer-MSG-TESSEL system to provide maps of sensible and latent heat

IRRIMED LANDSAF WORKSHOP, 8-10 March, LISBON WAGENINGEN UR

WAGENINGEN UNIVERSITEIT
WAGENINGEN UR

Examples

Date:

11/15/2002

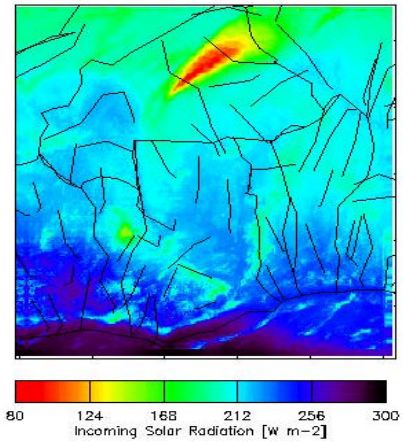

WAGENINGEN UNIVERSITEIT
WAGENINGEN UR

Examples

Date:

11/15/2002

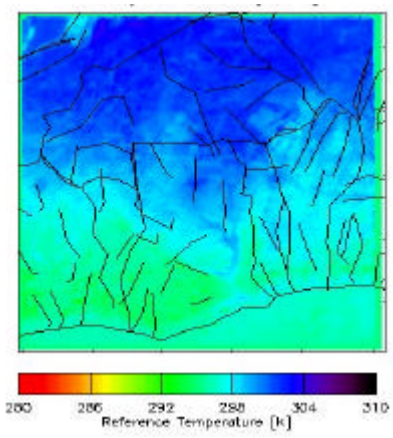

WAGENINGEN UNIVERSITEIT

Examples

Date:

11/15/2002

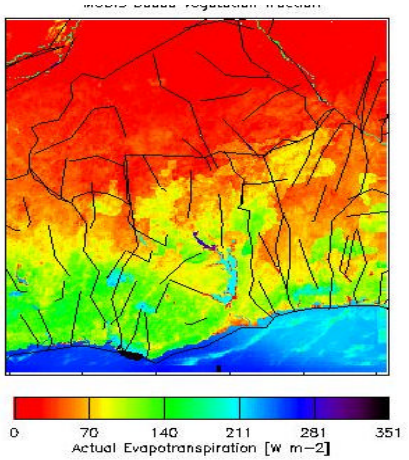

WAGENINGEN UNIVERSITEIT

Shortcomings of baseline algorithm

- No variation for the crop factor k_c
- No interception from vegetation
- No bare soil evaporation

- Larger errors emerged on days with daily mean wind speed of more than 3 m s^{-1}.

IRRIMED LANDSAF WORKSHOP, 8-10 March, LISBON WAGENINGEN UR

WAGENINGEN UNIVERSITEIT

Enhanced baseline algorithm

- Variation for the crop factor based on USGS
- Interception from vegetation
- Bare soil evaporation

- => absolute need for precipitation estimation

(if possible daily resolution)

WAGENINGEN UNIVERSITEIT

Extra Input I: landcover from USGS database

$$E_{opt} = k_c E_{ref}$$

- 1-km nominal spatial resolution
- based on 1-km AVHRR data
- spanning April 1993 through March 1994
- averaged to our resolution as is by now
- Additional check with standard deviation

Crop factor is based on literature and on local measurements

IRRIMED LANDSAF WORKSHOP, 8-10 March, LISBON WAGENINGEN UR

WAGENINGEN UNIVERSITEIT

Interception from vegetation

$$I = VF \times \min(P, aP + b)$$

P = Precipitation/day

a, b = parameters determined by vegetation and rainfall characteristics

WAGENINGEN UNIVERSITEIT

Bare soil evaporation

Occurance in two stages

- First stage is energy limited

$$E_{s1} = E_{opt}(1 - VF)$$

- Second stage is exfiltration limited

$$E_{s2} = s[t^{0.5} - (t-1)^{0.5}]$$

  - s = desorptivity
  - t = days elapsed since the day following rainfall

IRRIMED LANDSAF WORKSHOP, 8-10 March, LISBON WAGENINGEN UR

WAGENINGEN UNIVERSITEIT

Extra Input II: RI

- African Rainfall E

Based on 4 di

1) Daily GTS rain gauge d
2) AMSU microwave sate
3) SSM /I satellite rainfall
4) GPI cloud-top IR tempe

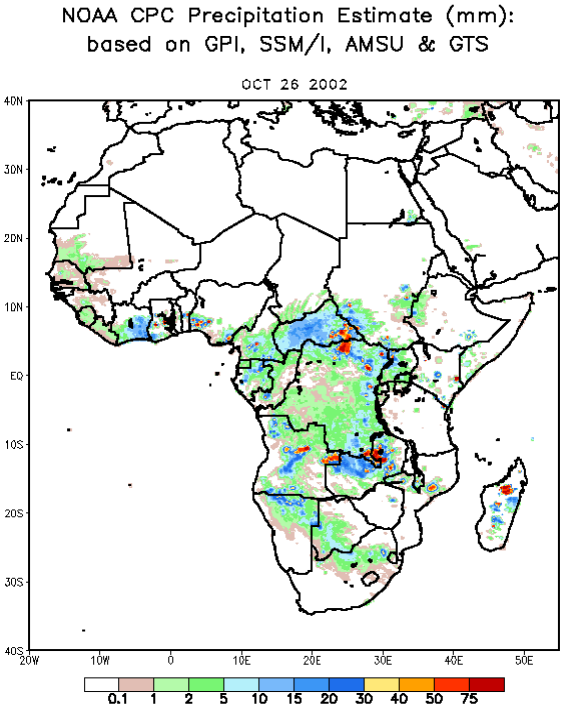

IRRIMED LANDSAF WORK

WAGENINGEN UNIVERSITEIT

RFE adopted to West Africa

- Selection of interest area
- Downscaling of original gridded information of 0.1° to 0.04°
- Additional check for precipitation with actual cloud cover obtained from Meteosat

WAGENINGEN UNIVERSITEIT
WAGENINGEN UR

XLAS output

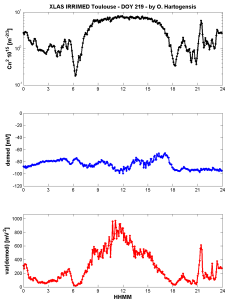

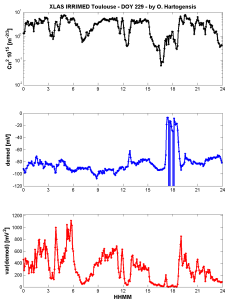

THE USE OF MSG LAND SAF PRODUCTS IN THE FRAME OF THE MARS CROP YIELD FORECASTING ACTIVITIES – FIRST RESULTS

Bettina Baruth, Catalin Lazar, Fabio Micale, Antoine Royer, Peter Viaene*

Joint Research Centre, European Commission
I- 21027 Ispra (Italy)
Name.surname@jrc.it
*VITO - Flemish Institute for Technological Research
B-2400 Mol (Belgium)
Name.surname@vito.be

ABSTRACT

The paper describes the work so far performed to evaluate the information content of LSA SAF products in order to ingest them in our Crop Yield Forecasting system. This is done with the purpose either to replace existing sources of parameter derivation (meteo-stations) or to fill gaps in the observed data.

A short description of the operational MSG chain to adapt the LSA SAF products to our needs is given and first evaluation results for the LST product are shown.

1. INTRODUCTION

The MARS (Monitoring Agriculture with Remote Sensing) – Stat Action of the AGRIFSIH Unit at the JRC runs since 1993 an operational activity on the analysis of crop growth condition assessment and crop yield expectations and forecasts. The system in place to analyse crop growth and providing forecasts is the so called MARS Crop Growth Monitoring System (CGMS) which is embedded in a series of additional tools and services called MARS Crop Yield Monitoring System (MCYMS). It has the objective to provide precise, accurate, scientific, traceable and independent forecasts for the main crops yields at EU level.

The CGMS itself consists of three levels:

- weather monitoring,
- crop simulation taking into account the actual weather situation and
- final yield forecasting.

Results are regularly published in form of monthly bulletins containing analysis, forecasts and thematic maps on crop yield expectations.

All these levels are supported by the use of remote sensing data up to different extents but the use MSG data is a novelty as for the first time meteorological parameters are covered by RS data within the MCYFS. So far only meteorological data from stations has been used for weather monitoring and derivation of agro-meteorological and crop growth parameters. As a consequence the use of the MSG data is seen as a possibility to enhance the meteorological infrastructure and derive the needed parameters for the crop growth model (e.g. Tsum) and / or to directly ingest RS data like radiation in crop growth model. Moreover the data can be regarded as an independent source of information to confirm crop growth indicators and forecasts using derived vegetation state indicators (like FVC) and weather indicators.

2. MSG DATA PROCESSING

As the MSG-SEVIRI data is not the first remote sensing data used in an operational context within the MARS crop yield monitoring system certain preconditions concerning area of interest, projection system, time steps and so on had to be fulfilled to be in accordance with our other RS products, namely from SPOT VEGETATION and NOAA-AVHRR. This implied the set-up of a specific production chain based on the LSA SAF products.

2.1 MSG processing chain

This automated chain has been set-up for the reception of the LSA SAF products, and for the further processing, archiving and delivery of the final results. The main steps of the processing chain can be summarized as follows:

- Regularly and automated ftp download of new data from LSA SAF, if enough data is available to process a whole day
- Unpack the compressed data,
- Conversion of HDF5 to ENVI format and
- For the LSA SAF products which are not delivered as daily values i.e. DSSF, ET, LST and solar duration, daily values are calculated using the available images for a period covering the interval from 6:00 UTC for a particular date to 6:00 UTC the day after.
- Determine the number of cloud free hours for the product ‘sunshine duration’

- The products with daily values are still in satellite projection and have to be projected to INSPIRE-LAEA for the output framing. For MSG the output resolution was fixed at 5 km.
- Calculate regional unmixed means (RUM) for the database to exploit spatialized profiles (like DSSF for non-irrigated arable land within a certain NUTS region over time).

Acronym	Product Contents	DT	CP	Available	IMG	DB	QLK
DSSF	Solar radiation	I	1	Sept. 2005	+	+	+
-	Solar duration	B	1	Oct. 2005			
SC	Snow Cover	B	1	Sept. 2005	+	+	+
AL	Surface Albedo	B	1	Sept. 2005	+	+	+
LST	Land Surface Temperature	I	1	Sept. 2005	+	+	+
ET	Evapotranspiration	B	1	Not yet	+	+	+
FVC	Fraction of Vegetation Cover	B	1	June 2006	+	+	+
LAI	Leaf Area Index	B	1	June 2006	+	+	+
fAPAR	Fraction of Absorbed PAR	B	10	Not yet	+	+	+

Table 1: Overview of the MSG products.

Data type (DT) can be either 8-bit byte (B) or 16-bit short integer (I). The compositing period (CP) is 1 or 10 days IMG – image data, DB – regional means DB filled, QLK: quick-look.

The chain as presented above also produces decadal images (in addition to the daily products) for all LSA SAF products. For the LST products the minimum and maximum values for the decadal products are based on the average daily values and not the daily minimum and maximum respectively. For all decadal images quicklooks are also produced. An example is given in Figure 1.

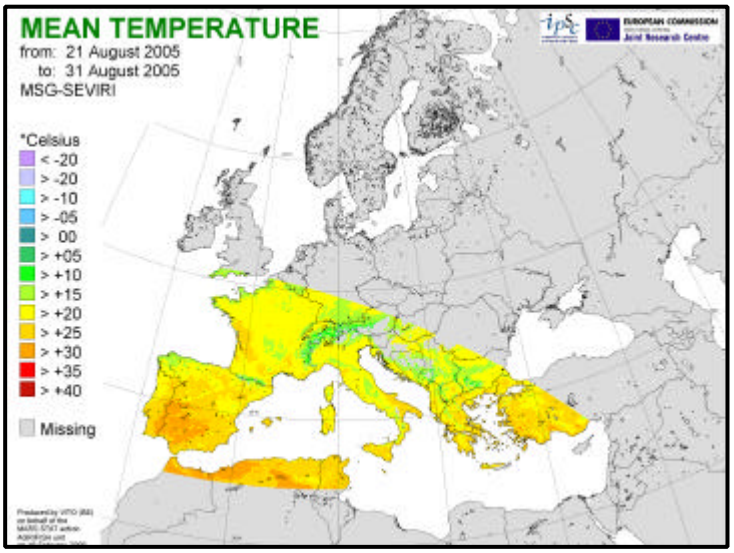

Figure 1: Quicklook of the decadal product mean temperature as an output of the processing chain

2.2 MSG data availability

Since the operational download of LSA SAF products started in the course of 2005 we had to cope with fluctuating data availability. The LST, DSSF, SC and AL became available for download in the course of 2005 and have been downloaded regularly during the first 6 months of 2006 by the processing chain implemented at VITO. Since May of this year 2 vegetation products, the fractional

vegetation cover (FVC) and the leaf area index (LAI) have become available for download from the ftp site as well.

The Figure 2 presents the data availability since January 2005 for the DSSF, LST, Snow Cover and Albedo products. It appears that the situation has somewhat stabilized with some excellent months such as February and April 2006 where nearly no data was lost and months during which as the year before on average 15 % of data were lost.

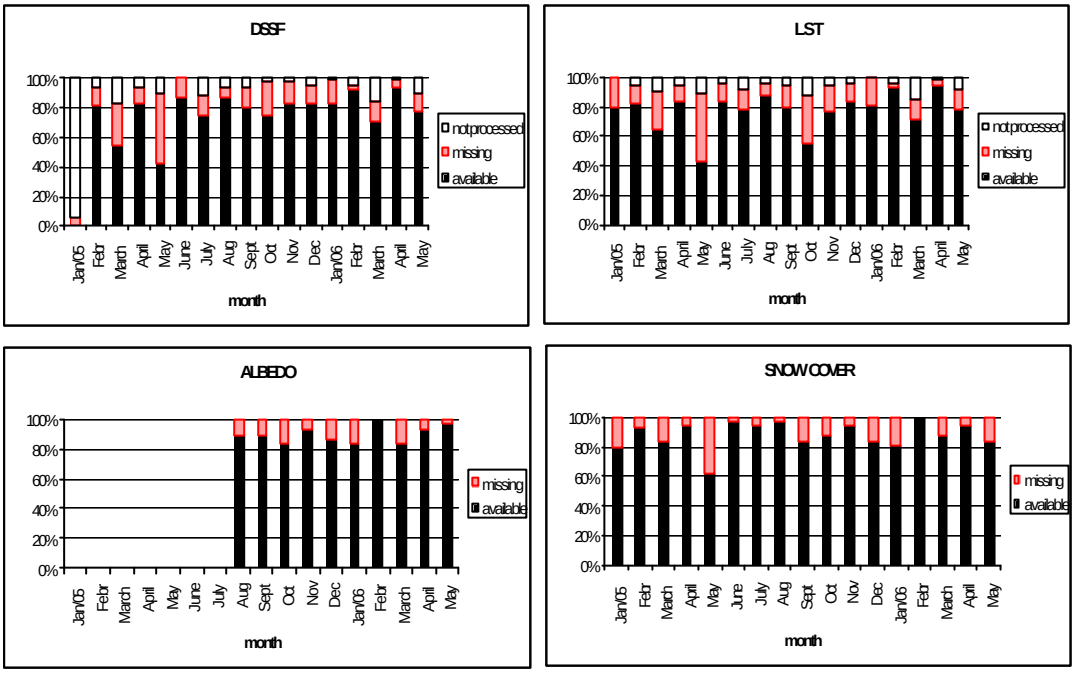

Figure 2: Data availability since January 2005 for the DSSF, LST, snow cover and albedo products.

3. USE OF LSA SAF PRODUCTS

The CGMS-model uses primary inputs like rain, temperature, radiation and wind. The input data come from meteorological-stations and is received daily. Information is gathered and interpolated to a 50 km * 50 km grid. However, these stations are not always distributed homogeneously, data delivery is not always regular and some inputs like radiation are particularly difficult to acquire. As an alternative these parameters can be derived from MSG.

For our purposes the meteorological products delivered by the LSA SAF can be divided into two groups:

1. Data that serves to enhance our existing meteorological infrastructure and that allows us to derive the needed parameters for the spatialized CGMS crop growth model (LST average to replace Tsum as a derived parameter from air temperature measurements). We see here the possibility to:
    - Fill gaps within the station data,
    - Increase the density of the observation network and cross-checking
    - Have a (Back-up) solution in case of degrading meteorological networks, e.g. new MS

2. Data that can be directly ingested into our CGMS crop growth model as it is a required parameter. This is the case for:
    - DSSF
    - Sunshine duration and
    - Snow presence

Moreover the data can be regarded as an independent source of information to confirm crop growth indicators and forecasts using derived vegetation state indicators (like FVC).

4. LAND SURFACE TEMPERATURE

For the LST product first evaluation test were made in order to answer the question if we find a correlation between LST data and our station data. That would allow us to use MSG data for the summing up of daily average temperature to the crop specific Tsum (withTsum = ?daily average temperature > specific crop threshold). This value drives the phenological stages of the crops in the crop growth model.

As the two derived temperatures are based on different measurement approaches (air temperate – point measurement 2 m above ground and Land Surface measurement as an integrated measurement for a pixel of the radiated skin temperature) and different average methods are used (Meteo AVG = (MAX+MIN) / 2; MSG AVG=true avg) the two measurements can not be simply exchanged within the system. Moreover time zoning effects have to be taken into account.

For the comparison the MSG pixel which coincides with the meteo-station location was selected and pixel values were read out. In total 1027 of the meteo-stations were covered by MSG data, this corresponds to 40 % of the meteo stations within EU 25 that are available within the MCYFS.

4.1 Spatial and temporal data availability

LST temperatures are only derived if the viewing angle is between the nadir and 57.5° resulting mainly in coverage of southern Europe. Moreover in case of cloudiness values are not retrieved as clear sky observations are required. These two conditions cut down data availability quite significant.

Analyzing 262 daily images from 2005 for the LST data at 12:00 (Figure 3) it can be noticed that a sufficient coverage with LST values can be obtained for Spain, large parts of Italy, Greece and Turkey. Non sufficient number of observations is reached for France, here for most of the area only 20 -30 % of the available information. As we have a dense net of meteorological stations over Europe delivering air temperate it is challenging to compete against it based on this restricted availability of information. But nevertheless the good coverage of Spain is promising, as this is one of the countries with a lower density of meteorological stations within our network.

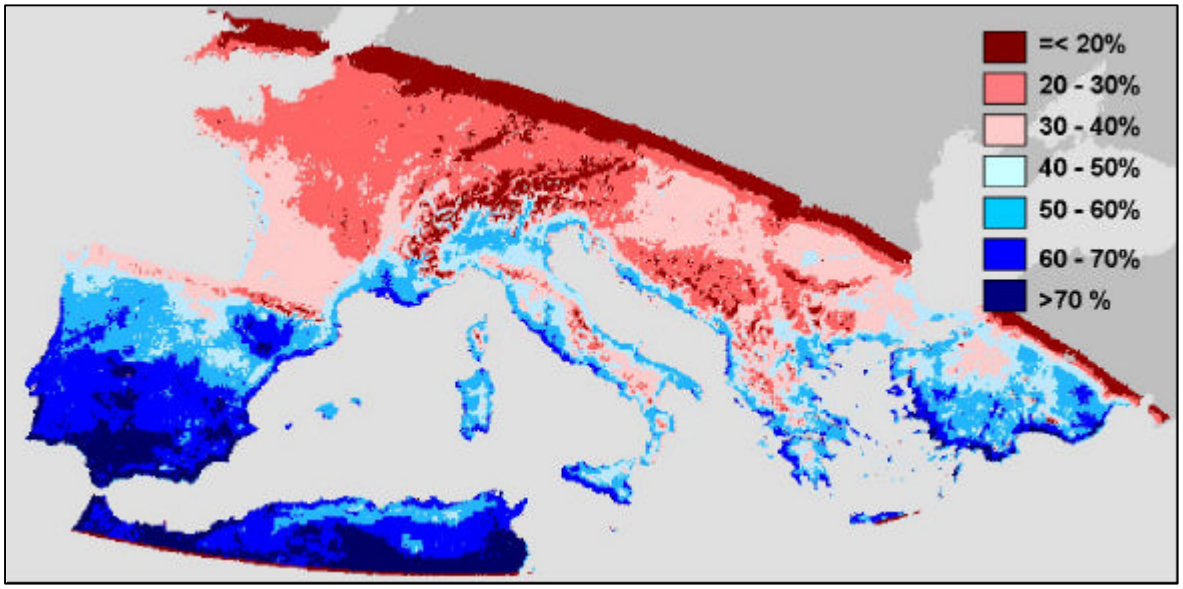

Figure 3: Processed MSG pixels in percent of 262 daily images in 2005 of LST 12:00 UTC

4.2 Comparison with air temperature from station data

Based on the available LST information comparisons with the air temperature data were performed. This was done for the 12:00 UTC data, for the daily average and min and max values by looking at single stations, group of stations, distinct geographical regions and the whole set.

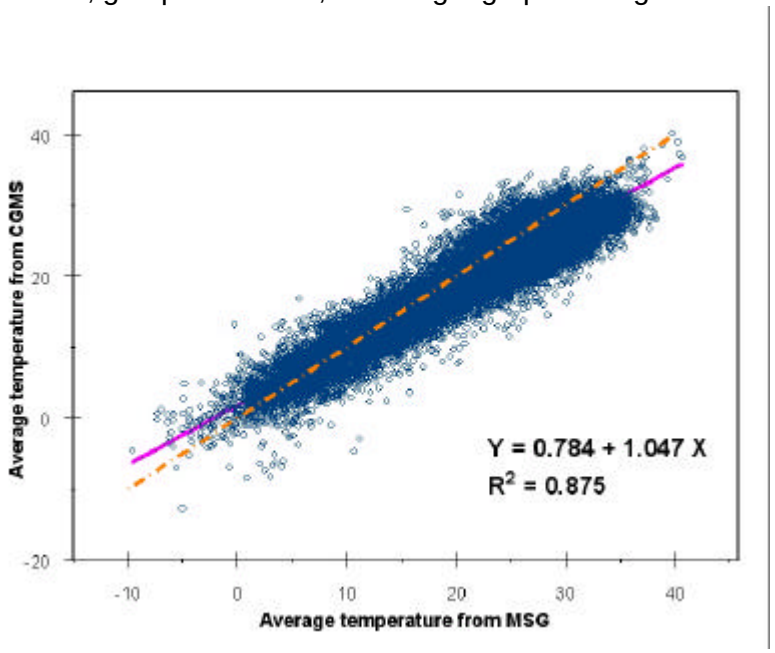

Figure 4: Average temperature for all stations. Comparison between LST and air temperature from 1027 meteo-stations for 262 days in 2005

Figure 4 shows the comparison of the average LST and average air temperature for 1027 meteo stations for 262 days in 2005. The slope is close to 1 and with a R2 of 0.875. Looking at maximum, 12 00 h and minimum data we see less variance explained, but this analysis revealed that linear relationships between the daily temperatures provided by MSG and observed temperatures at station level (CGMS) are able to explain a large part from total variation:

- 65% for temperature at 12:00h and maximum temperature

- 75% for minimum temperature and
- 87% for average temperature

Starting from this overall picture behaviour over time was analysed. It was noticed that in the cold months we had less absolute deviations from the air temperature and less variance within the data. On the other side the month of August for the maximum values showed an R^2 of 0.4033 and for y= 0.36 x + 15.28. This is a consequence of the increasing differences between air temperature and skin temperature under hot weather conditions.

As a next step we looked at the spatial distribution of the data. Figure 5 shows the absolute daily average differences in degree for all stations in 2005 for the maximum temperature as well as for the minimum temperature. We see fewer differences for the minimum temperature but high average differences for the maximum temperature, especially in Spain with a range between 10 and 20 degrees. Moreover the differences seem to be country specific. On average lower differences for France than for the Iberian Peninsula are appearing.

Furthermore station behaviour versus LST data was inspected by choosing a set of meteo-stations with at least 100 days covered by MSG observations in 2005, in average 172 days were covered. In fact out of the 1027 active stations covered by the LST footprint only 247 stations had more than 100 observations at 12:00 UTC throughout 2005. Figure 6 shows the regression coefficient for MIN, MAX, 12:00 and AVG of these selected stations.

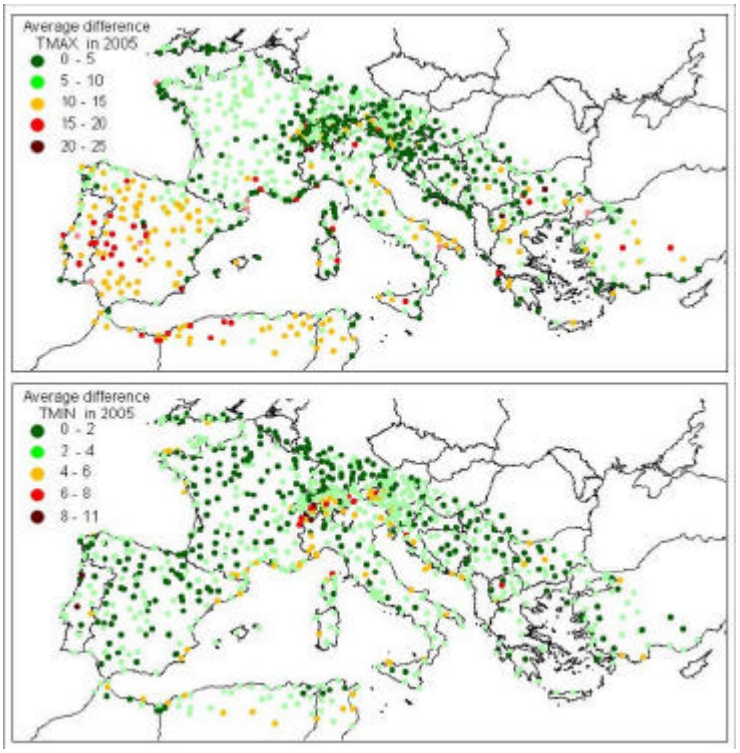

Figure 5: Absolute daily average differences in degree in 2005 for all stations, maximum value and minimum value

The less optimal correlation for the minimum and the maximum temperature seems to be compensated when working with the average value. Again the high correlation for the average temperature is confirmed and evenly distributed within the stations well covered by MSG observations. On the contrary a set of stations with very low regression coefficients for every product can be detected (e.g. south-east Sicily, east Tunisia) surrounded by stations with good

results. But in general looking at station level it can be noticed that there are slope differences from station to station but in general high R2 values and many stations with the slope close to 1.

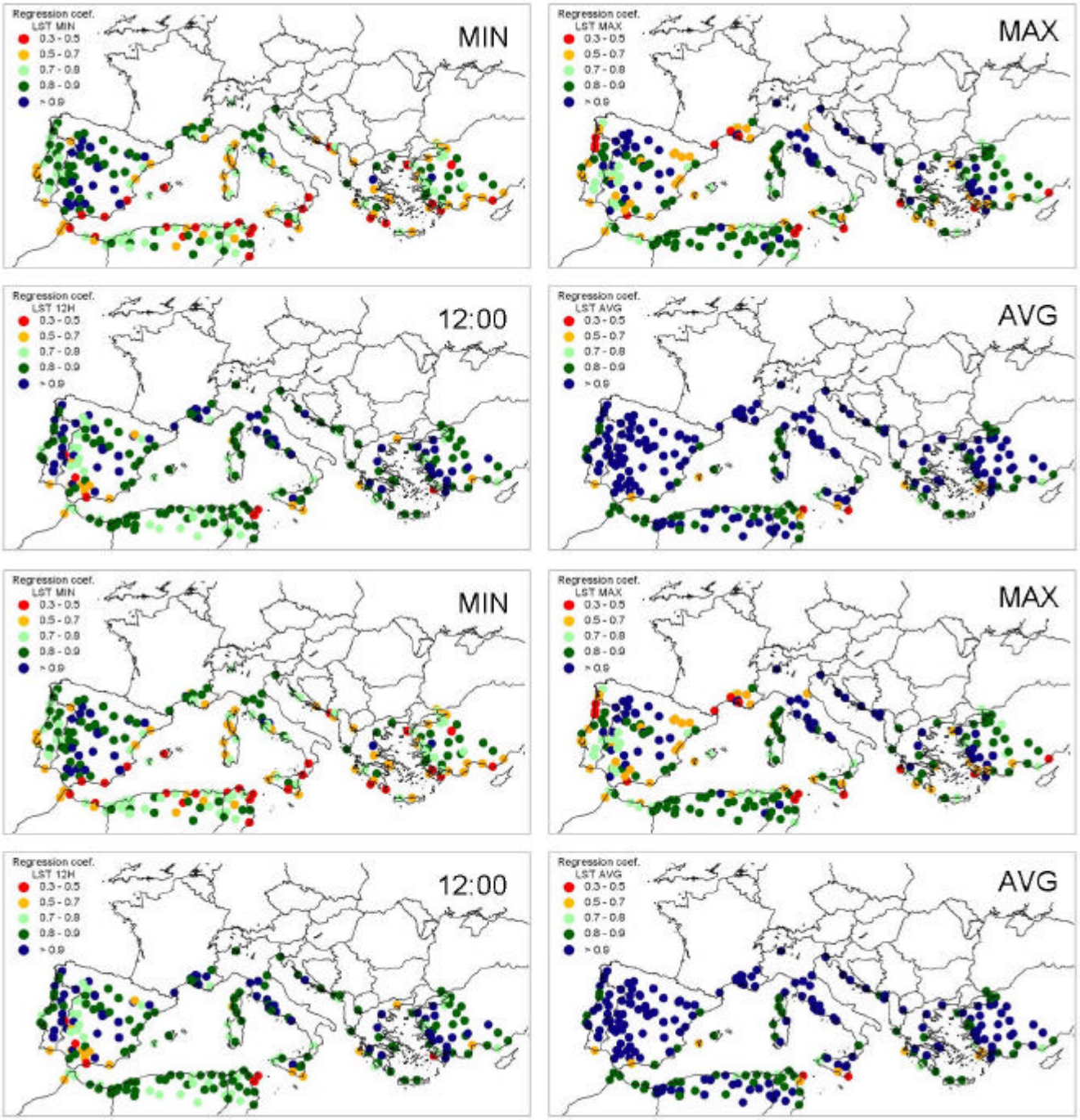

Figure 6: Regression coefficient for the correlation between LST and air temperature at station level over most complete stations (at least 100 LST measurements per station in 2005)

5. OUTLOOK

As the average temperature is the required input data for CGMS the overall good correlation especially in the southern countries is an encouraging finding. Results suggest that local regressions (for each station) are preferable to general ones or to the regressions for the sub-sets for latitude, longitude, altitude or country. This will allow taking the differences in slope from station to station into account. Special emphasis will be given to stations that are located within invariant surfaces (e.g. airport stations) as this surface is easier to model than vegetation behavior and has a more constant relationship over time with the air temperature. This should be done on a monthly basis as shown by the analysis.

The next steps will also include further evaluation of the information value of the LST product by performing a T-sum comparison concerning different crop thresholds (0°C, 7.8°C) based on derived MSG data and an interpolated grid weather comparison.

MSG data will further be used as an independent data source to evaluate the behaviour of the "suspicious stations", as a consequence they might be excluded for the future.

Concerning Snow Cover and Radiation, products of main importance for the direct ingestion, similar analysis will be performed. Snow Cover data was used already this spring as an independent source from the observed weather data by defining delays of sowing due to adverse weather conditions.

6. REFERENCES

BECKER, F., LI, Z.L. (1990): Temperature-independent spectral indices in thermal infrared bands, Remote Sens. Environ., vol. 32, pp. 17-33.

GENOVESE, G. (ed.) (2004). Methodology of the MARS Crop Yield Forecasting System . Eur Rep 21291 EN/1-4.

LI, Z.-L., BECKER, F (1993): Feasibility of land surface temperature and emissivity determination from AVHRR data, Remote Sensing & Environ., vol. 43, pp. 67-85.

Product User Manuel – Land Surface Temperature, Version 1.3, 16. January 2006.

WAN, Z., DOZIER, J. (1989): Land surface temperature measurement from space: physical principles and inverse modeling, IEEE Trans. Geosci. Remote Sens., vol. 27, no.3, pp. 268-278.

INVESTIGATIONS OF LAND-ATMOSPHERE INTERACTIONS IN THE WEST AFRICAN MONSOON USING SATELLITE REMOTE SENSING

Phil Harris[1], Chris Taylor[1], Doug Parker[2], Richard Ellis[1]

[1]Centre for Ecology and Hydrology, Wallingford, U.K.
[2]Institute for Atmospheric Science, School of the Environment, University of Leeds, U.K.

Investigations of Land-Atmosphere Interactions in the West African Monsoon using Satellite remote Sensing

Phil Harris[1], Chris Taylor[1], Doug Parker[2], Richard Ellis[1]

[1]Centre for Ecology and Hydrology, Wallingford, U.K.
[2]Institute for Atmospheric Science, School of the Environment, University of Leeds, U.K.

Outline

- African monsoon
- Recent studies using Meteosat 7 and TRMM images
- Overview of AMMA programme 2005-2007
- Proposed use of Meteosat 8/LandSAF products

Climatology of West African Monsoon

- Warm and dry air and surface
- H > LE

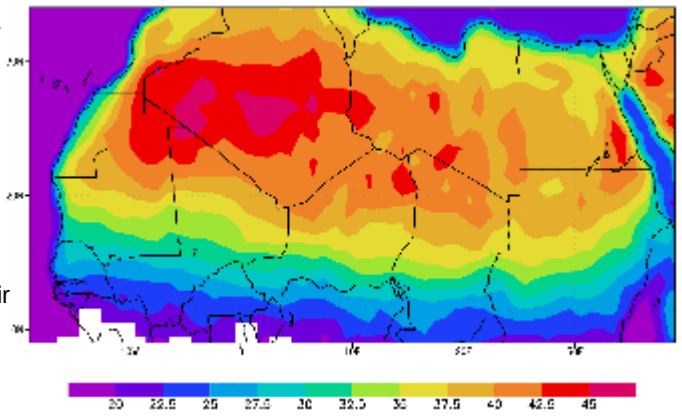

- Cool and moist air and surface
- LE > H

July-Sept 2000. Cloud-screened Meteosat 7 TIR

Variability in West African Monsoon

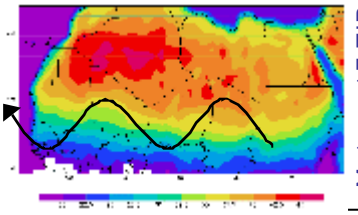

Meteosat 7 TIR

- 90% of Sahelian rainfall from meso-scale systems embedded in waves

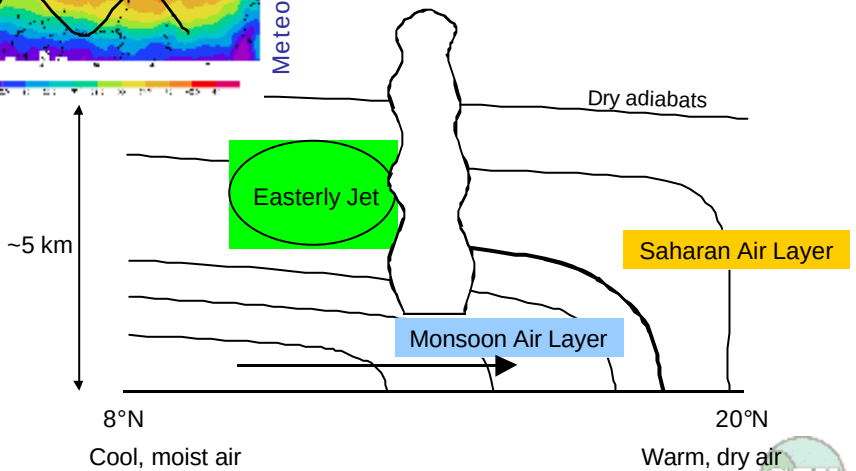

Land-Atmosphere Coupling Strength

Results from multi-model GLACE experiment
Koster et al, 2004*, Science.*

- Atmospheric models show strong coupling in West Africa during monsoon
- In arid Sahel, surface temperature and moisture anomalies closely related
- Need observations to assess how coupled system functions

West African Monsoon

JET2000 case study

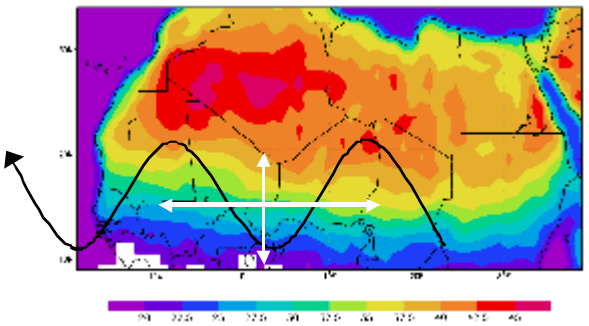

- Objective: sample lower atmosphere and boundary layer properties across easterly waves
- Continuous measurements of temperature, humidity, wind, radiation onboard aircraft
- Dropsondes every 0.5° lat. or lon.

JET2000

Impact of wet patches on properties of the PBL

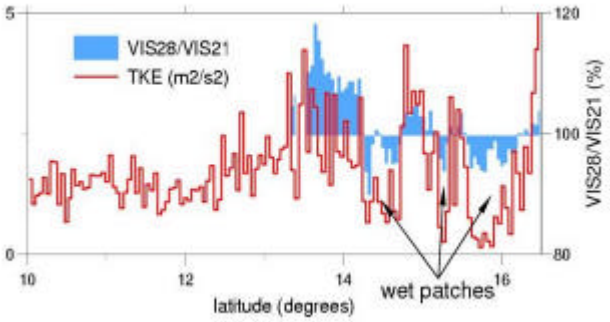

- Low level (950 m) flight in mid-afternoon
- PBL is more turbulent over dry soil due to large sensible heat flux

JET2000 Meteosat 7 images (11am)

Minimum TIR preceding 3 days

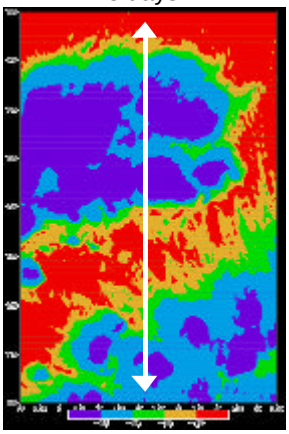

TIR 11 UTC flight day

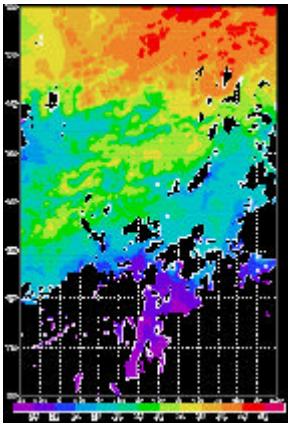

Visible 11 UTC flight day

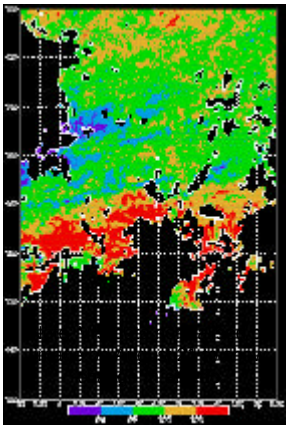

Low surface temperature and albedo pixels (blue/purple) indicate surface soil moisture from recent rain.

JET2000: subsequent cloud development

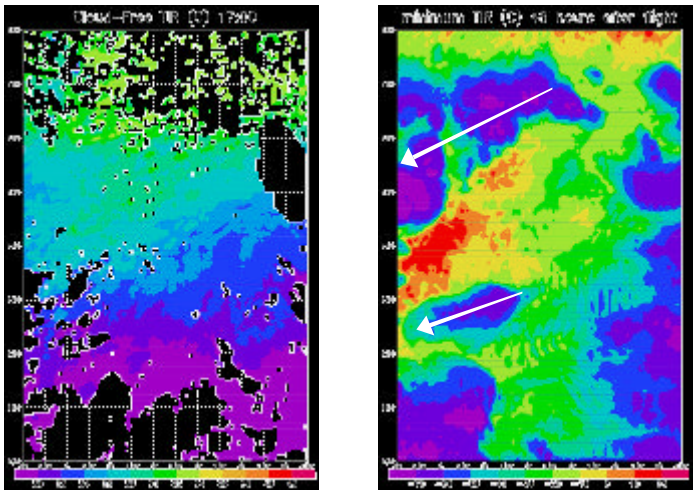

- Little afternoon cloud development over dry region
- Little storm initiation at meso-scale in following 2 days

Synoptic-Scale Interactions

Cloud-screened Meteosat 7 TIR temperature patterns

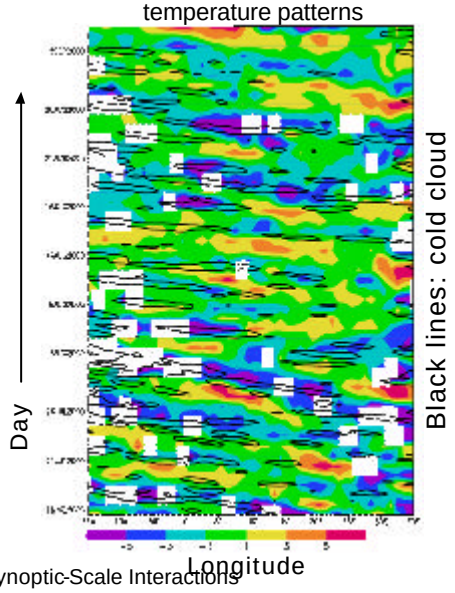

- Alternate warm and cool surface anomalies propogate westwards across the Sahel
- Cool surface features appear after rain
- Weather systems produce strong zonal variability in surface fluxes

Impact of Synoptic Surface Variability on Atmosphere

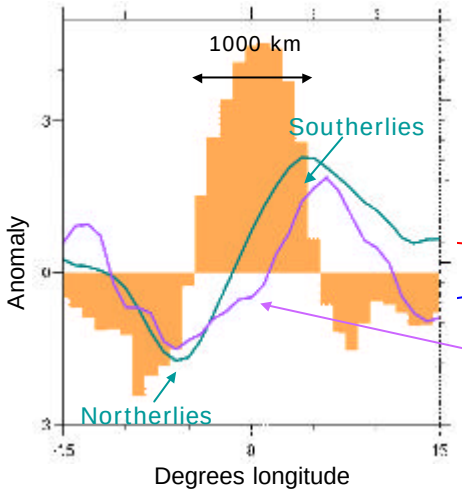

- Constructed composite "hotspot" from anomalies through 2000 wet season
- ECMWF operational analyses suggest,
  - Higher air temperatures
  - Lower surface pressure
  - Vortex develops
  - Subsequent cold cloud (rainfall) modulated

Taylor et al, 2005, *QJRMS*

Meso-scale interactions

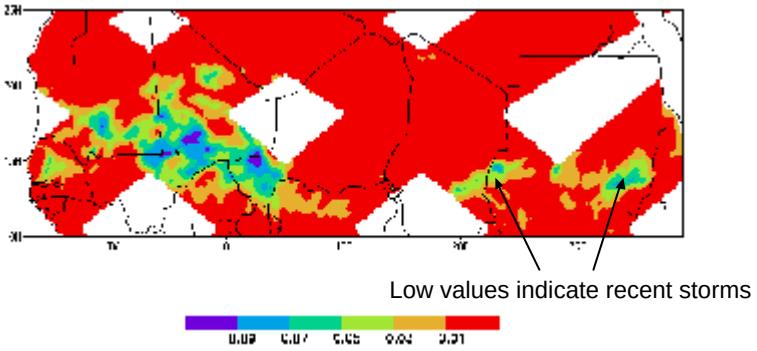

- Passive microwave data from TRMM
- Polarisation ratio at 10 GHz are very sensitive to soil moisture variations

Taylor and Ellis, 2006, *GRL*

Meso-scale interactions

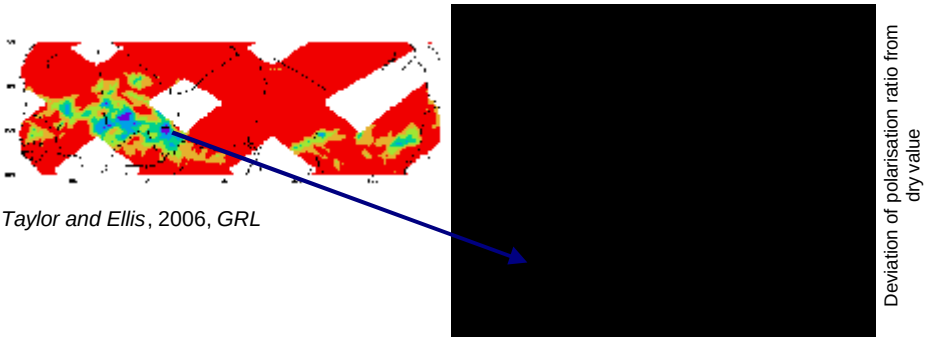

Taylor and Ellis, 2006, *GRL*

- Passive microwave data from TRMM
- Construct composite to,
  - Examine evolution of cloud field on subsequent day
  - Reduces influence of random component of cloud field
  - Wet and dry areas subject to same larger-scale forcing, differences are due to soil moisture

Meso-scale interaction: an individual case

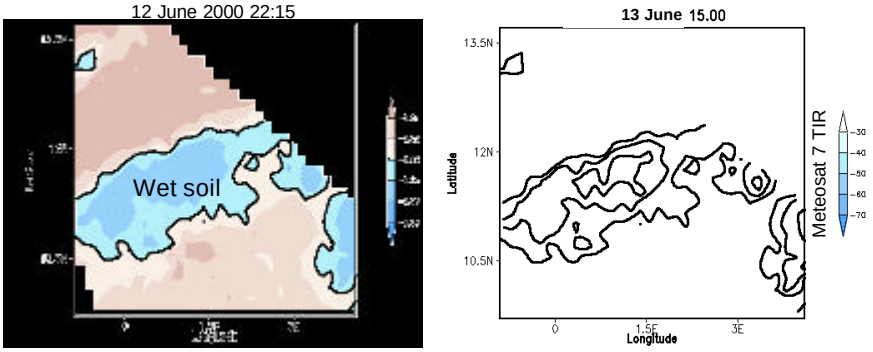

- In this single case, extent of convective system influenced by soil moisture
- Storms appear to “avoid” wet patch

Meso-scale interaction: composite of cases

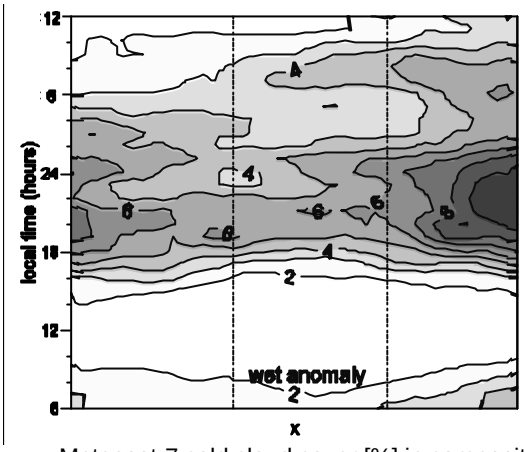

Meteosat 7 cold cloud cover [%] in composite (739 cases)

- Examined 108 cases manually
- Initiation over wet soil strongly suppressed (only 2% cases)
- Over 50% cases similar to example shown
- 33% reduction in evening cold cloud over wet patch
- Even clearer signal for small (<200 km) cloud systems
- Suggests a negative soil moisture – precipitation feedback

Different year, different satellite, same behaviour!

Soil moisture derived from AMSR-E

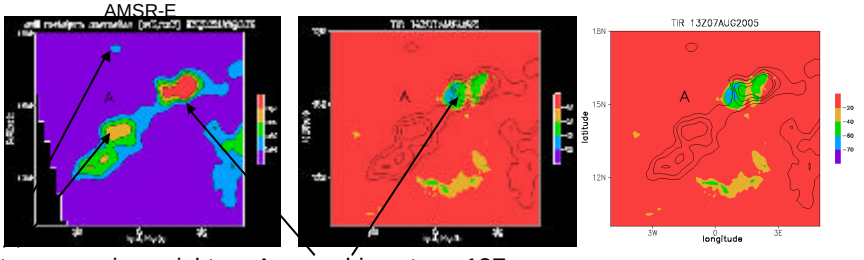

Storms previous night

Approaching storm 13Z

66 mm at Agoufou (c.f. 401 mm annual mean)

To understand impact of feedback on seasonal time scale, important to analyse events

Summary of these studies

- Synoptic-scale
  - Surface anomalies linked to westward propagation of African easterly waves
  - Land-atmosphere interaction provides a positive feedback on wave propagation
- Meso-scale cool, moist patches
  - Inhibit development of organised convective systems initiated within 100 km (negative feedback)
  - Enhance mature convective systems (positive feedback)

AMMA: African Monsoon Multidisciplinary Analyses

- Aim: to improve our understanding of the West African Monsoon and its *physical, chemical and biological* environment
- Observation
  - Satellite remote sensing, multi-aircraft flights, radio- and tethered-sondes, flux station network
- Observation periods
  - Long OP (2001-2010), Enhanced OP (2005-2007), Special OP (2006, 6 week blocks)
- Modelling
  - GCM, forecast, mesoscale, land-surface, atmospheric chemistry, vegetation

AMMA programme

AMMA SOP flight planning

- Unlike JET2000, we will target AMMA flights over transects of heterogeneous surface moisture
- These will be guided by anomalies in Land SAF LST product as a proxy for surface moisture

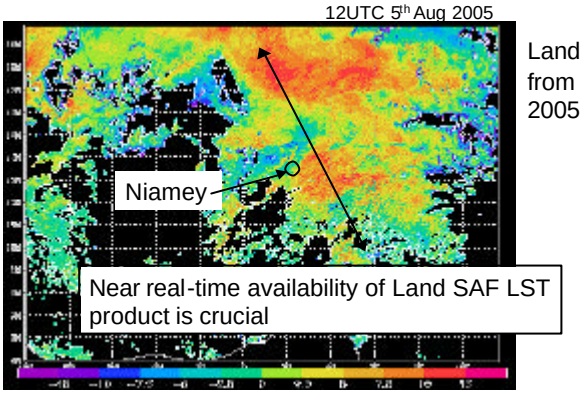

Land SAF LST anomaly from 12 UTC 1st - 9th Aug 2005 mean

AMMA EOP modelling

- Little is known about the seasonal cycle of surface energy fluxes through the monsoon
- Modelling and observation studies indicate that land-atmosphere interactions important for monsoon dynamics
- We will provide analyses of surface state/fluxes across West Africa through the EOP
- Some of this work done as part of ALMIP (see A. Boone presentation), we will extend this to include assimilation of Land SAF LST product to nudge precipitation forcing
- Currently investigating suitable method for this…

Summary

- Observations from aircraft confirm utility of satellite estimation of meso-scale surface variability in the Sahel
- We have begun exploiting this to investigate land-atmosphere interaction in the region
- AMMA programme will provide many opportunities to use MSG and Land SAF products, and compare with in-situ data over range of scales

APPLICATIONS OF THE LAND-SAF DOWNWELLING RADIATIVE FLUX PRODUCTS WITHIN AMMA

A. Boone

CNRS-GAME
MOANA/GMME/CNRM, Météo-France
42 avenue G. Coriolis, 31057 Toulouse, France

ABSTRACT

West Africa has been subjected to extreme climatic variability over the last half century. These radical fluctuations in the regional hydro-meteorological regime have had dramatic socio-economic consequences for the people and the relatively agrarian-dominated economies of this region. The AMMA (African Monsoon Multidisciplinary Analysis) project was organized in recent years with the main goal of obtaining a better understanding of the intra-seasonal and interannual variability of the west-African monsoon (WAM). Land-atmosphere coupling is theorized to be significant in this region, therefore a high priority goal of AMMA is to better understand and model the influence of the spatio-temporal variability of surface processes on the atmospheric circulation patterns and the regional water cycle. To meet this goal, high quality data with a high spatio-temporal coverage over a large region is needed. Certain LAND-SAF products are key to meeting this requirement. Several applications of LAND-SAF products within AMMA in terms of coupled land-atmosphere and “offline” (decoupled) surface modelling are presented.

1. INTRODUCTION

West Africa has been subjected to extreme climatic variability over the last half century, with relatively wet years during the 50s and 60s being followed by a much drier period during the 70s-90s. These radical fluctuations in the regional hydro-meteorological regime correspond to one of the strongest inter-decadal signals observed for the entire planet over the last century, and they have had dramatic socio-economic consequences for the people and the relatively agrarian-dominated economies of this region. Seasonal to inter-annual prediction of the West-African monsoon (WAM), which is the main precipitation driving mechanism, has therefore become a research topic of importance. However, difficulties modeling the African monsoon arise from both the paucity of observations at sufficient space-time resolutions, and because of the complex interactions of the attendant processes at various temporal and spatial scales between the biosphere, atmosphere and hydrosphere over this region. Land-atmosphere coupling is theorized to be significant in this region of the globe (e.g. Koster et al. 2004). At the small scale, these interactions have an impact on convective cells within mesoscale storm systems, while at the regional scale they influence the position of the Intertropical Convergence Zone and the African East Jet through a significant meridional surface flux gradient (Taylor et al., 1997), thus improvement of the modeling of the related processes is critical.

One of the main goals of the AMMA (African Monsoon Multidisciplinary Analysis) project is to improve the understanding and prediction of the WAM on both relatively short (sub-diurnal to several days) and long (seasonal) timescales in order to improve sustainable water management and related activities over western Africa. This is being addressed through a prolonged period of intensive and enhanced multi-year field observations, and through the development and use of various remote sensing-based products, notably those from the SAF projects (OSI and LAND). To this end, a multi-scale land-surface model atmospheric and land surface parameter forcing database is being constructed using a variety of sources; NWP forecast data, remote sensing products (primarily those from the SAFs and AMMA-SATellite) and local scale observations. The various data inputs used to comprise the forcing at three distinct spatial scales is shown in Fig. 1.

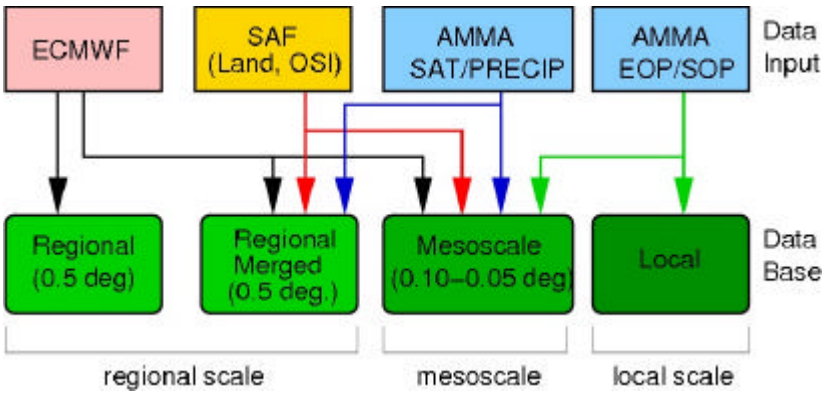

Figure1: The atmospheric forcing data base consists in three spatial scales. The various input data sources are shown (upper panels). The LAND-SAF surface radiative flux products starting in 2005 (and the OSI-SAF products for 2004) are critical components for both the regional scale and mesoscale forcing datasets.

One of the main applications of this database which is currently underway is to use the data to drive a host of land surface, vegetation and hydrological models over a range of spatial scales (local to regional) in order to gain better insights into the attendant processes. This is being done under the auspices of the AMMA Land surface Model Intercomparison Project (ALMIP), and through the development of an African Land Data Assimilation System (ALDAS). The offline

simulated land surface state will have several potential uses. For example, the simulated states and the LAND-SAF surface radiative fluxes will be compared to Global Climate Model (GCM) output within the WAMME project. In addition, the offline simulated "realistic" soil moisture state will be used to investigate it's impact on the iniation and subsequent life cycle of convection over west Africa through mesoscale atmospheric modelling studies.

2. APPLICATIONS OF THE SAF RADIATIVE FLUX PRODUCTS

2.1 ALMIP

The improvement of models and the understanding of land-atmosphere processes obviously depends upon quality forcing and evaluation data. Numerous field experiments have been done over the years with the objective of improving the understanding of the link between the land-surface and the atmosphere. Some examples of some of the most published studies are HAPEX-MOBILHY (André et al. 1986), FIFE (Sellers et al. 1988), BOREAS (Sellers et al. 1997), and Cabauw, the Netherlands (Beljaars and Bosveld 1997). These data sets have been of great value in terms of Land Surface Model (LSM) development, evaluation and intercomparison studies. In particular, the Project for the Intercomparison of Land-surface Parameterization Schemes (PILPS: Henderson-Sellers et al. 1993) has increased the under standing of LSMs, and it has lead to many improvements in the schemes themselves. In Phase-2 of PILPS (Henderson-Sellers et al. 1995), LSMs have been used in so-called "off-line mode" (driven using prescribed atmospheric forcing), and the resulting simulations have been compared to observed data.

The first attempt by PILPS to address LSM behavior at a regional scale was undertaken in PILPS-2c (Wood et al. 1998). LSM forcing data was constructed from a combination of atmospheric model and field data. The GSWP (Phase 1: Dirmeyer et al. 1999) was an "off-line" global-scale LSM intercomparison study which produced 2-year global data sets of soil moisture, surface fluxes, and related hydrological quantities. This project relied heavily on remotely sensed data from the ISLSCP Initiative I (Meeson et al. 1995; Sellers et al. 1995), along with atmospheric model data. The Rhone-AGGregation LSM intercomparison project (Rhone-AGG: Boone et al. 2004), differed from the aforementioned studies primarily because the impact of changing the spatial scale on the LSM simulations was investigated which was made possible by higher spatial resolution forcing data (based mostly on observational data).

The AMMA Land surface Model Intercomparison Project (ALMIP: deRosnay et al. 2006) is part of the AMMA-EU (European Union) and API (Action Programmée Interorganisme: AMMA French program. It is being conducted at CNRM (Centre National de Recherches Météorologiques: National Center for Meteorological Research) and CESBIO (Centre Etudes Spatiales de la BIOsphère: Center for the Study of the Biosphere from Space), in Toulouse, France. The strategy proposed in AMMA to develop a better understanding of fully coupled system is to break the various components into more manageable portions which will then provide insight into the various important processes. The first step is to begin with the land surface in off-line or uncoupled (without atmospheric feedbacks) mode. The idea is to force state-of-the-art land surface models with the best quality and highest (space and time) resolution data available in order to better understand the key processes and their corresponding scales (as was done in the aforementioned intercomparison studies). ALMIP is relying heavily on remotely sensed products for key atmospheric forcing fields (notably the precipitation and shortwave downwelling radiative flux). The regional and mesoscale model domains are shown in Fig. 2.

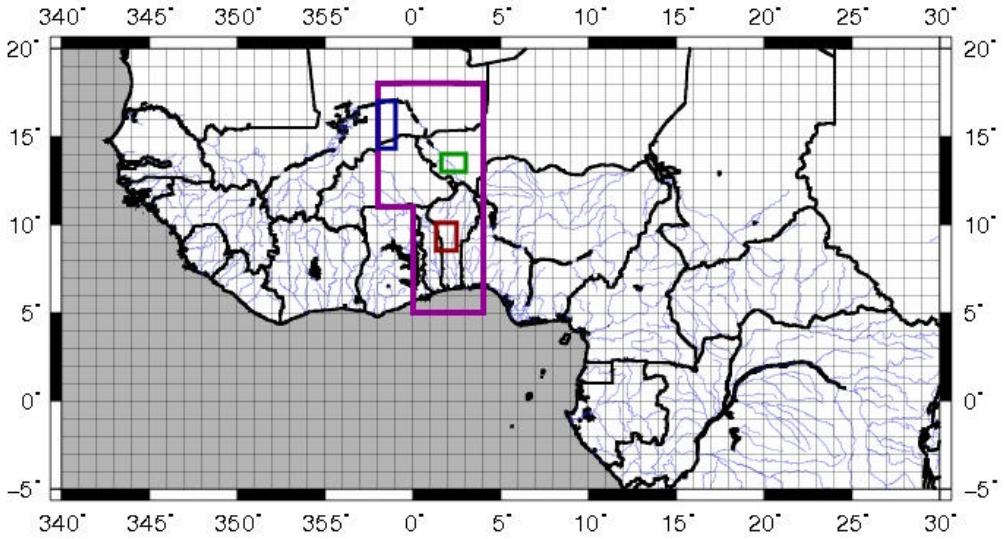

Figure 2: The regional scale domain used in ALMIP. The LAND-SAF radiative fluxes are aggregated to the approximate resolution of the NWP model over this domain (0.5 degrees). The radiative fluxs are used at a 0.1 degree resolution over the mesoscale or CATCH domain (which is shown: the large box extending from –2 to 4 degrees east longitude). The high resolution radiative fluxes will also be compared to observed values located within three smaller intensive mesoscale sites (with numerous local scale observations): from north to south they are located in Gourma in Mali, Niamey in Niger, and Oueme in Benin.

In order to address the known limited ability of LSMs to simulate the surface processes over western Africa, ALMIP has several objectives. Two of these objectives are being addressed using the SAF fluxes: to examine how the various LSM respond to changing the spatial scale (notably the meso and regional scales owing to the high spatial resolution of the the SAF and AMMA-SAT products), and to develop a multi-model climatology of ``realistic'' high resolution (multi-scale) soil moisture, surface fluxes, and water and energy budget diagnostics at the surface (which can only be accomplished in such a data-sparse region through the use of satellite-based products). Indeed, the ECMWF model simulated monsoon has the tendency to remain too far south (note that this is not a problem unique to the ECMWF model: most operational NWP models and GCMs have difficulties simulating various aspects of the WAM). In order to simulate a more realistic surface state, ancillary data are required over a large domain, especially for the precipitation and incoming shortwave radiation.

A comparison between the ECMWF and LAND-SAF monthly average downwelling shortwave radiative flux at the surface (SWdown) is shown in Fig. 3. The control dataset uses the ECMWF model output to drive land surface models (Fig. 3a.), while the merged forcing dataset incorporates the LAND-SAF SWdown (Fig. 3b). It can be seen that the LAND-SAF SWdown is considerably lower in the north-western and north-central parts of the domain, consistent with increased cloudiness (presumably indicating a farther northward extension of the monsoon). This same tendency is also seen in the MSG-based EPSAT precipitation product (Chopin et al. 2004). The merging of EPSAT with OSI-SAF in 2004 resulted in a significant change in the meridional soil moisture (and surface flux) gradient (which theorized to be one of the key components modulating the intensity of the monsoon). The same response is expected for 2005 using the NWP-EPSAT-LAND-SAF merged forcing dataset.

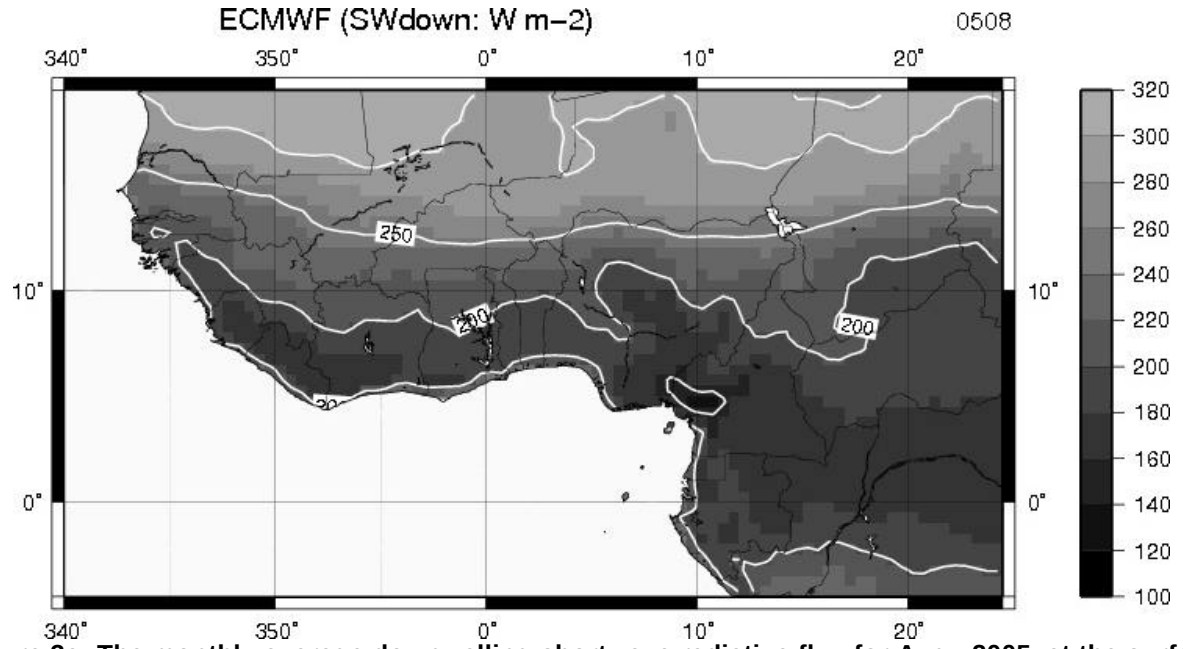

Figure 3a: The monthly average downwelling shortwave radiative flux for Aug., 2005, at the surface from ECMWF.

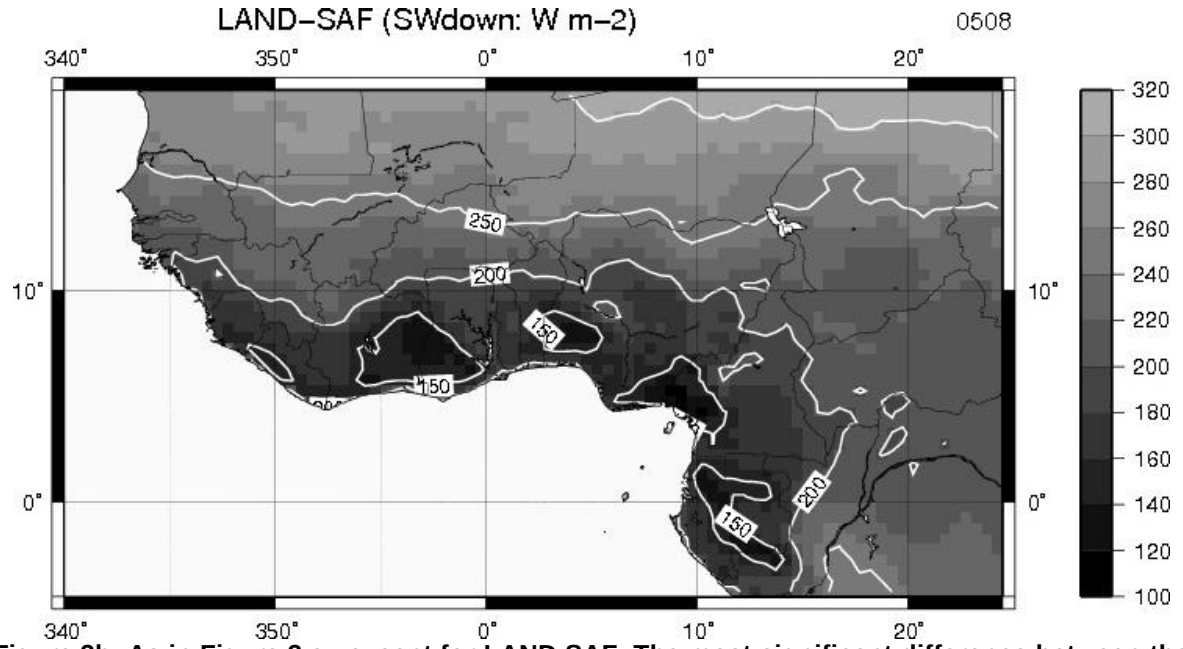

Figure 3b: As in Figure 3.a., except for LAND-SAF. The most significant difference between the LAND-SAF and ECMWF SWdown is the farther northward extension of significant cloudiness (and possibly precipitation) in the SAF product.

2.2 Towards ALDAS

The African Land Data Assimilation System (ALDAS) is currently under development. It builds upon the infrastructure developed within ALMIP, but in contrast it will operate in the quasi real-time mode. Currently, EPSAT precipitation and LAND-SAF downwelling radiative products have been re-gridded and reformatted by IPSL and Medias, France, for direct use by land surface and atmospheric models. These forcing data will again be merged with a combination of observational

and NWP data to produce atmospheric forcing for a group of land surface schemes in order to derive a realistic land surface state for NWP model initialization. This is similar to the methodology used within the Land Data Assimilation System (LDAS: Rodell et al. 2004). In addition, both observations and additional remotely-sensed data will be directly assimilated into the system (such as in the European LDAS, ELDAS: Meetschen et al. 2004). Testing will begin near the end of 2006 and into 2007.

2.3 Coupled surface-atmosphere studies

The off-line simulated soil moisture and surface fluxes over west-Africa will be used for several land-atmosphere coupled actions: two AMMA-related examples are discussed herein.

At CNRM, the soil moisture simulated of the ISBA land surface model (Noilhan and Mahfouf, 1996) in Aug., 2005, will be used to explore the impact of changing the soil moisture initial condition on short term forecasts using the French mesoscale meteorological model MesoNH (Lafore et al. 1998) within the contact of the "Dry Run" modelling exercise. One of the main goals of the Dry Run is to learn more about the predictability of the WAM. One experiment within the context of the Dry Run is to use the off-line simulated soil moisture to determine how much it influences both the initiation and subsequent development of convection and it's spatial and temporal distributions.

The simulated surface states and the LAND-SAF products themselves will be used within the international project West African Monsoon Model Evaluation (WAMME, Y. Xue, UCLA, B. Lau, NASA-GSFC, and K. Cook). The support of WAMME by GEWEX is based on the project's potential ability to break new ground in monsoon systems research with the objective to unravel the effect of aerosol-monsoon water cycle interaction in monsoon systems around the world. Since the West African monsoon variability is strongly affected by external forcings and their interactions, WAMME will necessarily encompass vegetation-ocean-atmosphere-aerosol interactions and is an interdisciplinary project. An ensemble of GCMs will simulate several years which overlap with the period covered by ALMIP. The simulated soil moisture states and surface fluxes will then be compared to the off-line simulated values. In addition, the GCM simulated downwelling solar and radiative fluxes will be compared to the LAND-SAF product. A first workshop is scheduled for Spring, 2007.

3. SUMMARY

One of the main goals of the AMMA is to obtain a better understanding of the intra-seasonal and interannual variability of the west-African monsoon (WAM). A key process is the interaction between the land and the atmosphere, which is theorized to be significant over this region, especially in terms of the soil moisture memory (and it's feedback with the atmosphere through surface fluxes). The first step towards improving understanding of the coupled land-atmosphere system is to begin with the land surface in off-line or uncoupled mode. The idea is to force an ensemble of state-of-the-art land surface models with the best quality and highest (space and time) resolution data available in order to better understand the key processes and their corresponding scales. To meet this goal, atmospheric forcing data are needed to drive land surface models, but NWP models have some inherent difficulties in terms of simulating the WAM. It is therefore of utmost importance to use ancillary data with high spatial and temporal coverage, which is a need that can only be addressed using remotely-sensed data. The two key variables driving land surface processes are the precipitation and the solar radiative flux, the latter of which is being provided by the LAND-SAF project from 2005 onward. Note that the LAND-SAF downwelling longwave radiative flux is also being used.

The multi-scale land surface database being constructed at CNRM in conjunction with other laboratories, notably CESBIO and ECMWF, is to be used for many projects beginning near the end of 2006, and then beyond: several of them were discussed herein. It is obvious that these projects reply heavily on the LAND-SAF products, from model intercomparison studies such as ALMIP and WAMME, to the development of operational assimilation systems for improving real-time NWP forecasting (ALDAS).

4. ACKNOWLEDGEMENTS

I would like to acknowledge the hard work of the co-organizer of ALMIP, P. deRosnay, in addition to all of the members of the ALMIP working group, and the support of J.-P. Lafore. I would also like to acknowledge all of the hard work by the data providers, notably K. Ramage, R. Lacaze,, and F. Chopin (precipitation data). B. Geiger and D. Carrer (CNRM) have offered considerable assistance with respect to using the LAND-SAF downwelling radiative flux products. The land surface initialization within the Dry Run exercise is being done in collaboration with N. Ascencio of CNRM-Météo-France. Gratitude is also to be expressed to Y. Xue who has made an effort to incorporate elements of ALMIP into the WAMME project.

5. REFERENCES

ANDRÉ, J. C., J. P. GOUTORBE, AND A. PERRIER (1986): HAPEX\u2013MOBILHY: A hydrologic atmospheric experiment for the study of water budget and evaporation flux at the climatic scale. *Bull. Amer. Meteor. Soc*., **67**, 138-144.

BELJAARS, A. C. M., AND F. C. BOSVELD (1997): Cabauw data for the validation of land surface parameterization schemes. *J. Climate*., **10**, 1172-1193.

BOONE, A., F. HABETS, J. NOILHAN, D. CLARK, P. DIRMEYER, S. FOX, Y. GUSEV, I. HADDELAND, R. KOSTER, D. LOHMANN, S. MAHANAMA, K. MITCHELL, O. NASONOVA, G.-Y. NIU, A. PITMAN, J. POLCHER, A. B. SHMAKIN, K. TANAKA, B. VAN DEN HURK, S. VÉRANT, D. VERSEGHY, P. VITERBO AND Z.-L. YANG: The Rhone-Aggregation Land Surface Scheme Intercomparison Project: An Overview. 2004, *J. Climate*, **17**, 187-208.

CHOPIN, F., J. C. BERGES, M. DESBOIS, I. JOBARD, AND T. LEBEL (2004): Multi-scale precipitation retrieval and validation in African monsoon systems. 2nd International TRMM Science Conference, 6-10 Sept., Nara, Japan.

DEROSNAY, P. A. BOONE, A. BELJAARS, AND J. POLCHER (2006): AMMA Land-Surface modeling and intercomparison projects. *GEWEX News*, February, **16** (1), 10-11.

DIRMEYER , P. A., A. J. DOLMAN, AND N. SATO (1999). The Global Soil Wetness Project: A pilot project for global land surface modeling and validation. *Bull. Amer. Meteor. Soc*., **80**, 851-878.

HENDERSON-SELLERS, A., A. J. PITMAN, P. K. LOVE, P. IRANNEJAD, AND T. CHEN (1995). The project for inter-comparison of land-surface parametrization schemes (PILPS): Phase 2 and 3. *Bull. Amer. Meteo. Soc*., **76**, 489-503.

KOSTER, R. D., P. A. DIRMEYER, Z. GUO, G. BONAN, E. CHAN, and Co-authors (2004). Regions of strong coupling between soil moisture and precipitation. *Science*, **305** (5687), 1138-1140.

LAFORE, J. P., J. STEIN, N. ASENCIO, P. BOUGEAULT, V. DUCROCQ, J. DURON, C. FISCHER, P. HEREIL, P. MASCART, J. P. PINTY, J. L. REDELSPERGER, E. RICHARD, AND J. VILA-GUERAU DE ARELLANO (1998): The Meso-NH Atmospheric Simulation System. Part I: Adiabatic formulation and control simulations. *Annales Geophysicae*, **16**, 90-109.

MEESON, B. W., and Coauthors (1995): ISLSCP Initiative I-Global Data Sets for Land-Atmosphere Models, 1987-1988, Vols. 1-5. NASA CD-ROM.

MEETSCHEN, D., B. VAN DEN HURK, F. AMENT, M. DRUSCH (2004): Optimized surface radiation fields derived from Meteosat imagery and a regional atmospheric model. *J. Hydrometeor*., **5**, 1091-1101.

NOILHAN, J., AND J.-F. MAHFOUF (1996): The ISBA land surface parameterization scheme. *Global Planet. Change*., **13**, 145-159.

RODELL, M., P. R. HOUSER, U. JAMBOR, J. GOTTSCHALCK, K. MITCHELL, C.-J. MENG, K. ARSENAULT, B. COSGROVE, J. RADAKOVICH, M. BOSILOVICH, J. K. ENTIN, J. P. WALKER, D. LOHMANN AND D. TOLL. (2004): The Global Land Data Assimilation System. *Bull. Amer. Meteor. Soc*., **85**, 381-394.

SELLERS, P. J., and Coauthors (1995): An overview of the ISLSCP Initiative I Global Data Sets. Vols. 1-5, NASA CD-ROM.

SELLERS, P. J., and Coauthors (1997): BOREAS in 1997: Experiment overview, scientific results, and future directions. *J. Geophys. Res*., **102**, 28731-28769.

TAYLOR , C. M., F. SAID, AND T. LEBEL (1997). Interactions between the land surface and mesoscale rainfall variability during HAPEX-Sahel. *Mon. Wea. Rev*., **125**, 2211-2227.

WOOD, E. F., D. LETTENMAIER, X. LIANG, D. LOHMANN, A. BOONE, S. CHANG, F. CHEN, Y. DAI, C. DESBOROUGH, Q. DUAN, M. EK, Y. GUSEV, F. HABETS, P. IRANNEJAD, R. KOSTER, O. NASANOVA, J. NOILHAN, J. SCHAAKE, A. SCHLOSSER, Y. SHAO, A. SHMAKIN, D. VERSEGHY, J. WANG, K. WARRACH, P. WETZEL, Y. XUE, Z.-L. YANG and Q. ZENG: The Porject for Intercomparison of Land-Surface Parameterization Schemes (PILPS) Phase-2c Red-Arkansas River Basin experiment: 3. experiment description and summary intercomparisons. 1998, *Glob. Plan. Change*, **19**, 115-139.

MAPPING SURFACE COMPONENTS OF THE HYDROLOGIC CYCLE THROUGH SEQUENTIAL ASSIMILATION OF LAND SURFACE TEMPERATURE

, F. Caparrini[1], F. Castelli[2], D.Entekhabi[3], L. Campo[2]

1 Eumechanos, Via La Marmora 22, 50121 Firenze (Italy)
2 Dipartimento di Ingegneria Civile, Università di Firenze (Italy)
3 Department of Civil and Environmental Engineering
Massachusetts Institute of Technology, Cambridge MA (USA)

ABSTRACT

Land Surface Temperature (LST) maps are used as the primary input in a sequential data assimilation system to estimate fields of surface hydrological components.

The assimilation scheme allows to simultaneously retrieve determinant parameters of land surface water and energy balance (turbulent transfer coefficient for heat fluxes, evaporative fraction, indices of soil moisture) with a very limited requirement of ancillary data and empirical assumptions. Besides the system-state (LST) observations, the assimilation system requires common data on meteorological forcing such as air temperature, wind-speed and incident solar radiation. Different contributions of soil and vegetation to the radiometric temperature are explicitly taken into account through a two-source formulation based on satellite vegetation indices.

Infrared channels from SEVIRI on board MSG-1 are now providing high resolution LST maps at unprecedented temporal rate and quality. An application of the above assimilation scheme is here presented with reference to such an improved data rate. The sensitivity study includes the use of MSG surface radiation products.

The study area includes the Tuscany region (approximately 20,000 Km^2 in Central Italy), where a large number of surface hydro-meteorological data are available from the regional network. Hourly maps of evapotranspiration an daily maps of surface moisture and vegetation indices are produced for an extended study period including summer and fall 2005, ensuring a large range of hydrological surface and atmospheric conditions. The sequential nature of the assimilation scheme allows the estimation of the surface hydrologic fields even during relatively prolonged periods with clouds covering the target area.

1. INTRODUCTION

Land surface temperature (LST) dynamics contains the "signature" of evapotranspiration and sensible heat fluxes from land surface to the atmosphere. For this reason, various studies use land surface temperature observations as the key to infer surface energy fluxes (Crow and Kustas, 2004).

LST measurements have been available from a variety of remote sensing instruments in the last two decades. Infrared channels from SEVIRI on board MSG-1 are now providing high resolution LST maps at unprecedented temporal rate and quality.

In the present study, LST maps are used as the primary input in a sequential data assimilation system (ACHAB, Assimilation Code for HeAt and moisture Balance) to estimate fields of land surface hydrological components. The assimilation scheme does not require empirical relations such as those that take G to be a given fraction of R_n (Bastiaanssen et al., 1998, Norman et al., 2000 and Boegh et al., 2002 among others). The approach estimates the partitioning between the surface energy balance components by minimizing the quadratic of errors due to any misfit of the dynamic surface energy balance and LST observations. This approach to evaporation estimation was introduced by Castelli et al. (1999), Boni et al. (2000 and 2001) and Caparrini et al. (2003).

Following such preliminary studies, further advancements of the model have been made, re-casting the variational assimilation system as a multi-scale framework where satellite LST estimates from several sensors can be assimilated (Caparrini et al., 2004a). Furthermore, a " dual-source" energy balance formulation has been introduced, where both the remotely sensed LST and the retrieved energy fluxes are treated as a combination of contributions from the canopy and from the bare soil surface.

The model has been first tested with GOES, SSM/I and AVHRR data over the US Midwest for a four-month warm-season period (Caparrini et al., 2004a). Comparison of the results with ground observations showed an overall consistency and a relevant sensitivity to the LST errors due to variable factors such as cloud cover.

An application of the dual-source assimilation scheme over the territory of Tuscany Region (Central Italy) is here presented with reference to the improved data rate provided by SEVIRI instruments.

LSA SAF LST maps for the period August-September 2005 are here used, while micrometeorological observations (radiation, wind speed, air temperature and humidity) were obtained from the Regional Agrometeorological network. Maps of heat fluxes from soil and vegetation and surface-related parameters were then retrieved from the assimilation model.
As a further application , the ACHAB assimilation model was run using also shortwave radiation products from LSA SAF, in order to evaluate the sensitivity to different sources of input data. Comparison between the retrieved energy fluxes and parameters using the two different radiation inputs is here discussed.

2. FORMULATION

The dual-source energy balance formulation follows Caparrini et al. (2004a). In this formulation the soil-vegetation system is schematised as a resistance network (Figure 1) that includes nodes at

the soil, the canopy leaves, the air within canopy and air above the canopy. The resistances are characterized through turbulent heat transfer coefficients C_{Hs} (for heat transfer from soil to air within the canopy) and C_{Hv} (from leaves to air within the canopy) where the surface conductance (inverse of resistance) is given by the heat transfer coefficient multiplied by wind speed at the corresponding level.

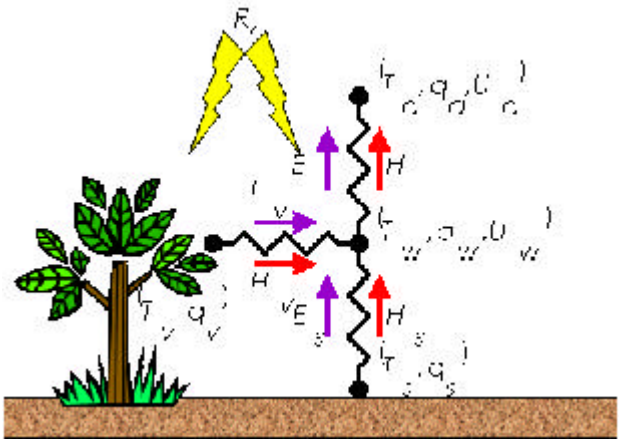

Figure 1: Schematics of dual-source (soil and vegetation) energy balance at the surface.

The heat transfer coefficients depend on surface heat transfer roughness length scale and atmospheric stability conditions. The latter effects can be taken into account by means of atmospheric stability correction functions expressed in terms of indicators such as Bulk Richardson number. The atmospheric correction function presented in Caparrini et al. (2004b) is used here.

Based on the heat transfer coefficients C_{Hs} and C_{Hv}, the sensible heat fluxes per unit of the contributing surface (soil and vegetation respectively) are given by:

$$H_s = rc_p C_{Hs} U_w (T_s - T_w) \tag{1a}$$

and

$$H_v = rc_p C_{Hv} U_w (T_v - T_w) \tag{1b}$$

where T_s, T_v are respectively soil and canopy temperatures, and T_w and U_w are the temperature of the air and the wind speed at a height within the canopy volume. The turbulent moisture flux is represented using the definition of evaporative fraction for soil:

$$EF_s = \frac{L \cdot E_s}{L \cdot E_s + H_s} \tag{2a}$$

and for vegetation:

$$EF_v = \frac{L \cdot E_s}{L \cdot E_v + H_v} \tag{2b}$$

where L is the specific latent heat of vaporization and E_s and E_v are the moisture fluxes per unit of contributing surface (soil and vegetation respectively). The denominator of evaporative fraction equations is also equal to the net available energy (R_n-G). Thus EF represents the fraction of available energy that is dissipated by latent heat flux in order to maintain energy balance. Higher values of evaporative fractions are generally associated to higher moisture availability in the soil and vegetation.

In order to take full advantage of the availability of sequences of remote LST estimates, that is to use also the temporal information in the assimilation procedure, a variational approach similar to the one of Caparrini et al. (2003) is used. This is based on the definition of a penalty function that incorporates, as a physical constraint through Lagrange multipliers, the surface energy balance described above. The estimated parameters are C_H , EF_v and EF_s.

The first term of the penalty function is given by a quadratic measure of the misfit between model predictions and LST observations. LST observations are radiometric temperature measurements which may be considered as a weighted sum of the contributions from soil and vegetation:

$$T_R = \left(f T_v^{\,4} + (1- f) T_s^{\,4} \right)^{\frac{1}{4}} \qquad (3)$$

The penalty function is to be minimized on the (C_H , EF_v , EF_s) parameters space under the model's constraint.

In order to be able to estimate more than one parameter by assimilating measurements on a single state variable, two main working hypotheses have been introduced:

- evaporative fractions EF_s and EF_v are kept constant during daytime hours, and may vary from one day to another; this hypothesis is supported by several studies (e.g. Crago, 1996);
- the bulk transfer coefficient is split in an equivalent 'neutral' part C_{HN} and a stability correction, empirically related to a bulk Richardson number R_B; the neutral part C_{HN} is the actual estimated parameter, and it is kept constant over a longer time scale (of the order of a month, during which the surface structural characteristics may be reasonably considered as invariant).

The assimilation scheme is then constructed with reference to two different integral time scales: the overall assimilation period of length D days, for which a single C_{HN} value is estimated for each state pixel j; a daily assimilation window during which EF may be considered constant and hence estimated for each pixel, independently for each day.

3. APPLICATION

The dual source ACHAB model has been implemented over the territory of the Tuscany Region, in Central Italy. The Regions covers an area of approximately 20,000 km^2 and is bounded by the Apennine mountains on the North, with maximum elevation reaching 1,300 m asl. Main land cover types are olive yards, vineyards, and forests in the mountain areas.

A fairly dense micrometeorological network is available in the area, which includes also a few stations that provide radiation measurements (Figure 2).

The period of study is late summer 2005 (August-September). During this period, generally characterised by high values of radiation forcing, several precipitation events of relatively high intensity occurred, in August especially in the northern part and in September more concentrated in the central part of the region .

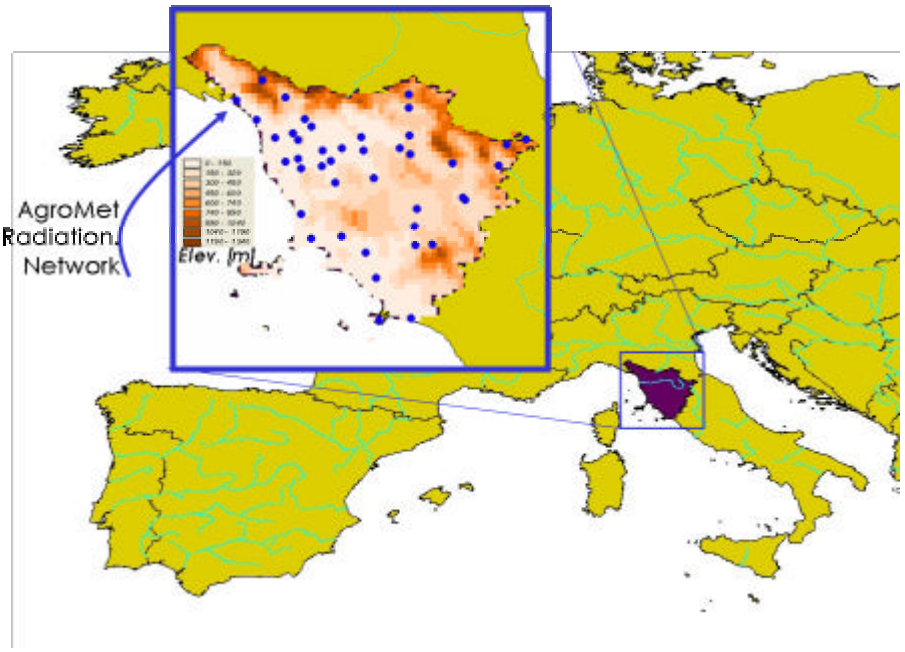

Figure 2: The study area (Tuscany Region). In the box, the location of stations from the agrometeorological network that provide also solar radiation measurements.

MSG-derived LST maps were retrieved for the period of study from the LSA SAF website. Radiation products were also obtained from the same source, in addition to the ones provided by the Regional Agrometeorological network. A sensitivity study on the effect of the use of the two different sources for radiation measurements is here also presented.

Table 1 summarises the data used in the assimilation scheme and their source. In the table, data in italics were not obtained from MSG products in the present study, but can be substituted with LSA SAF products (already available) in the further applications of the model.

Data	Source
LST	LSA SAF
Shortwave radiation	LSA SAF/ Regional Agrometeorological network
Longwave radiation	Computed from air temperature/humidity
Air temperature	Regional Agrometeorological network
Wind speed	Regional Agrometeorological network
Air humidity	Regional Agrometeorological network
LAI/ Fractional Vegetation Cover	Computed from AVHRR NDVI

Table 1: Sources of data used in the assimilation scheme. The variables in italics were not obtained from LSA SAF products in the present study but will be in future applications.

4. RESULTS

The assimilation scheme was applied first using the LST maps from LSA SAF while radiation, air temperature and wind speed data were obtained from the Regional Agrometeorological network.

Figure 3 shows the retrieved heat transfer coefficients for the months of August and September. Although the period of study is too short to appreciate a remarkable relationship with the phenological cycle, main topographical and land cover features are captured by the heat transfer coefficient patterns, and C_H values range between $10^{-2.7}$-$10^{-1.7}$ which corresponds to values commonly reported in the literature for this kind of landscape (Stull, 1988).

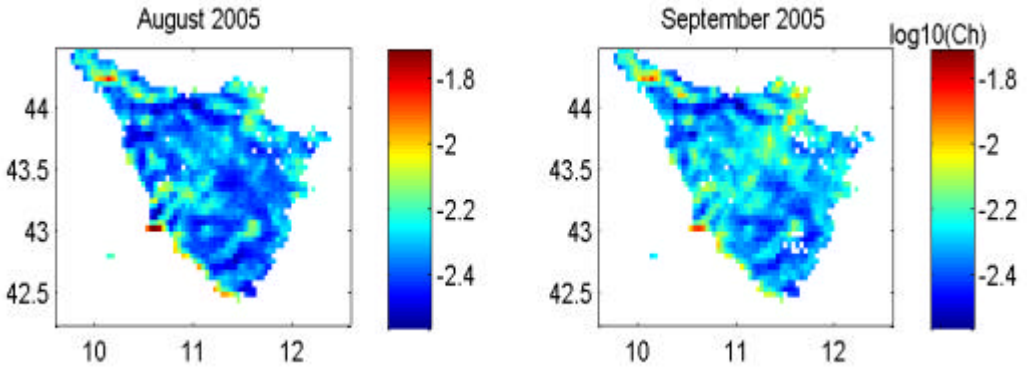

Figure 3: Bulk heat transfer coefficients (in log10) obtained from the assimilation scheme ACHAB

Figure 4 shows the monthly averages of evaporative fractions for soil (top panel) and vegetation (lower panel). Higher values of evaporative fractions are generally associated to higher moisture availability in the soil and vegetation. For instance in September higher values of EF_S are retrieved in the Central part of the basin, were more most precipitation events occurred. Evaporative fraction for vegetation has lower values compared to soil ones (expressing a tendency to preserve moisture flux) and very little spatial variability.

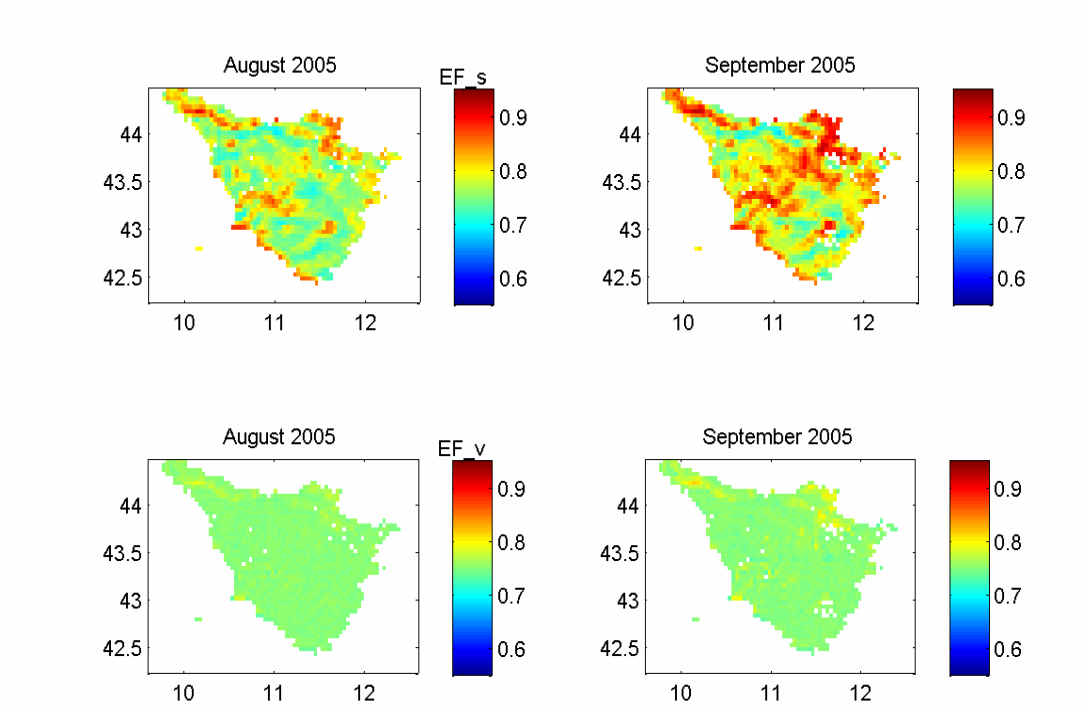

Figure 4: Monthly average evaporative fractions for soil (top panel) and vegetation (lower panel).

A major potential of the assimilation scheme, compared to other methods for heat flux retrieval from remote sensing, is in the fact that being a dynamic approach it allows to retrieve also the diurnal variability of surface energy balance components. Figure 5 shows the average diurnal cycle for the sensible and latent heat fluxes in soil and vegetation and the ground heat flux. It can be noticed that ground heat flux exhibits a diurnal variability that could not be captured with the usual "static" approaches that assume it as a fixed portion of net radiation.

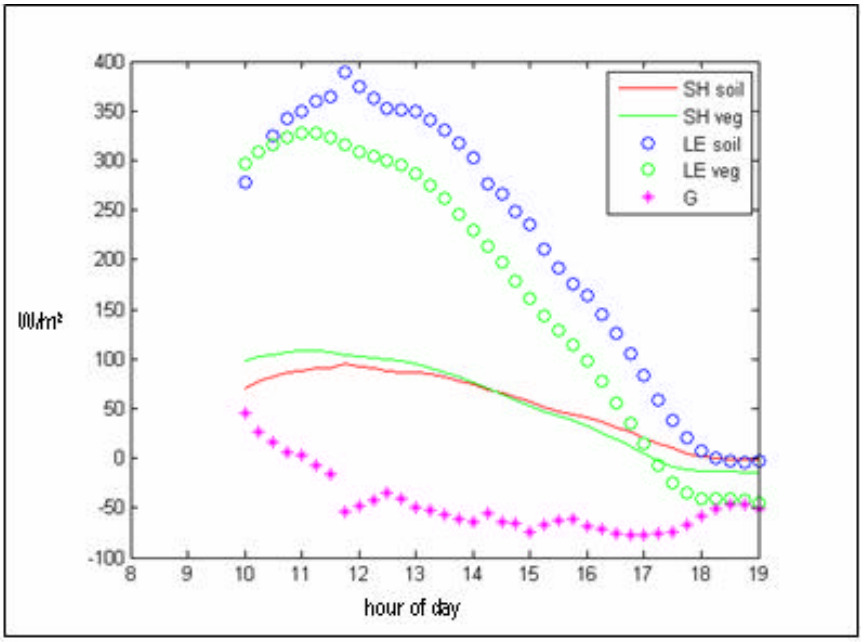

Figure 5: Average diurnal cycles of latent (LE) and sensible (SH) heat fluxes in soil and vegetation and ground heat flux (G).

As a further application , the ACHAB assimilation model was then run using shortwave radiation products from LSA SAF, in order to evaluate the sensitivity to different sources of input data.

Figure 6 shows the relative differences obtained for the month of August. Relative differences shown in the figure are calculated as:

$$Diff.XX\% = \frac{XX_{SAF} - XX_{ground}}{XX_{SAF}} \times 100 \quad (4)$$

where XX_{SAF} denotes the state/parameter XX estimated from the assimilation scheme with radiation from LSA SAF, while XX_{ground} is the same state/parameter estimated from the assimilation scheme with radiation data from the ground-based Regional Agrometeorological network.

It can be noticed that values of radiation data from LSA SAF are generally lower than those measured by the ground-based network (top left panel in Figure 6), with underestimation reaching 20%.

The variation in the values of the parameters (C_H and evaporative fractions) are generally contained within the range +/- 5%, but this causes however a high sensitivity in the retrieval of fluxes, especially peak values (for instance, lower panels in Figure 6 show differences in peak Latent Heat flux).

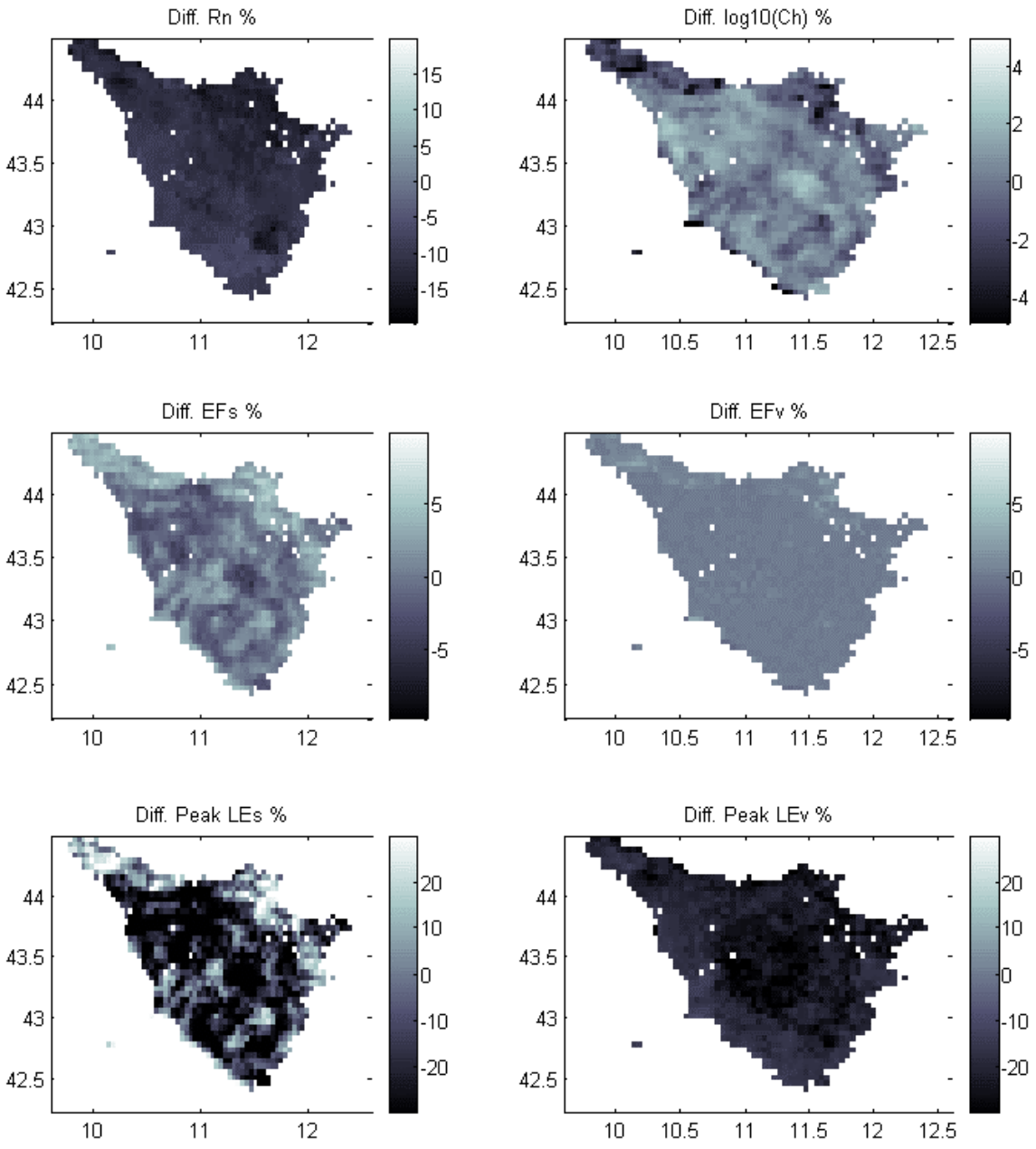

Figure 6: Relative differences between monthly averages of relevant variables obtained from the ACHAB assimilation model using radiation forcing from ground based stations and LSA SAF products. Relative differences are calculated as in Equation (4).

5. CONCLUDING REMARKS

An application of the variational assimilation scheme ACHAB over the territory of Tuscany Region (Central Italy) using LSA SAF land surface temperature products has been presented.

The dynamic approach to the computation of heat fluxes of the assimilation scheme makes it particularly suited to exploit the high temporal resolution provided by SEVIRI instrument. Although a sounder interpretation and validation of the results is not possible due to lack of surface measurements of heat flux, the preliminary results presented here show reasonable estimates of heat fluxes (both in terms of range of values and diurnal cycle) and surface control parameters.

A basic sensitivity study has also been conducted, comparing the results obtained using two types of radiation input: from the ground based network or from the LSA SAF shortwave radiation product. Results show a high sensitivity in the retrieval of heat fluxes, especially with regard to peak values.

Further applications under development on the same study area include the integration of SEVIRI LST maps with MODIS data. In fact, although only one type of LST maps was used in this study, the scheme has been developed in a multiscale/multisensor sense, i.e. it is formulated in order to assimilate LST inputs with different spatial and temporal resolutions. The use of MODIS (and other higher resolution thermal data) will allow to exploit both the spatial accuracy of such sensor and the high data rate of SEVIRI.
Other developments of the assimilation scheme are focused on its optimal integration with hydrologic models, coupling the surface energy balance implemented in ACHAB with the mass balance of hydrological budget in order to improve the estimation of soil moisture and evapotranspiration.

6. REFERENCES

BASTIAANSSEN, W. G. M., A. M. MENENTIA, R. A. FEDDESB, and A. A. M. HOLTSLAG (1998), A remote sensing surface energy balance algorithm for land (SEBAL): 1. Formulation, J. Hydrol., 212/213, 198– 212.

BOEGH, E., H. SOEGAARD, and A. THOMSEN (2002), Evaluating evapotranspiration rates and surface conditions using Landsat TM to estimate atmospheric resistance and surface resistance, Remote Sens. Environ., 79, 329– 343.

BONI, G., F. CASTELLI, and D. ENTEKHABI (2000), Sampling strategies and assimilation of ground temperature for the estimation of surface energy balance components, IEEE Trans. Geosci. Remote Sens., 39, 165–172.

BONI, G., D. ENTEKHABI, and F. CASTELLI (2001), Land data assimilation with satellite measurements for the estimation of surface energy balance components and surface control on evaporation, Water Resources Research, 37, 1713– 1722.

CAPARRINI, F., F. CASTELLI, and D. ENTEKHABI (2003), Mapping of land-atmosphere heat fluxes and surface parameters with remote sensing data, Boundary Layer Meteorology, 107, 605–633.

CAPARRINI F., CASTELLI F., ENTEKHABI D. (2004a), Variational Estimation of Soil and Vegetation Turbulent Transfer and Heat Flux Parameters from Sequences of Multi-Sensor Imagery, Water Resources Research, vol. 40, W12515, ISSN 0043-1397

CAPARRINI, F., F. CASTELLI, and D. ENTEKHABI (2004b), Estimation of surface turbulent fluxes through assimilation of radiometric surface temperature sequences, Journal of Hydrometeorology, 5, 145–159.
CASTELLI, F., D. ENTEKHABI, and E. CAPORALI (1999), Estimation of surface heat flux and an index of soil moisture using adjoint-state surface energy balance, Water Resources Research, 35, 3115–3126.

CRAGO, R. (1996), Conservation and variability of the evaporative fraction during the daytime, Journal of Hydrology, 180, 173–194.

CROW, W. T., and W. P. KUSTAS (2004), Utility of assimilating surface radiometric temperature observations for evaporative fraction and heat transfer coefficient retrieval, Boundary-Layer Meteorology 115(1): 105

NORMAN, J. M., W. P. KUSTAS, J. H. PRUEGER, and G. R. DIAK (2000), Surface flux estimation using radiometric temperature: A dual-temperature difference method to minimize measurement errors, Water Resources Research, 36, 2263– 2274.

STULL, R.N. (1988), An introduction to Boundary Layer Meteorology, Kluwer Academic Publisher, Dordrecht, The Netherlands.